

# **Phase Diagrams for Ceramists**

## **Volume IV**

**Robert S. Roth,  
Taki Negas, and  
Lawrence P. Cook**

Compiled at the **National Bureau of Standards**

**Geraldine Smith, *Editor***

**The American Ceramic Society**  
65 Ceramic Drive, Columbus, Ohio 43214

Printed in U.S.A.

## Ce-Zr-O

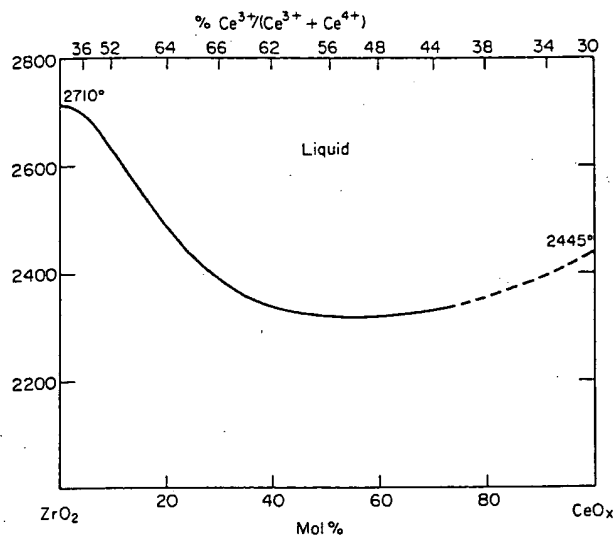


FIG. 5042.—System  $\text{ZrO}_2\text{-CeO}_x$ .  
A. Rouanet, *C. R. Hebd. Seances Acad. Sci., Ser. C.*, **266** [12] 908 (1968).

Ten compositions were formulated from  $\text{ZrO}_2$  and  $\text{CeO}_2$  of unspecified starting purity. Specific experimental details related to pretreatment of samples are not given but generalized methods can be found in Ref. 1. The liquidus curve was established using a solar furnace and thermal analysis methods in air.<sup>1,2</sup> Fused samples were quenched in water or in air, examined by powder X-ray diffraction, and reoxidized at  $800^\circ$  in air. Associated weight gains were used to calculate the degree of reduction of quenched liquids.

Figure 355 shows generalized subsolidus relations for the system  $\text{ZrO}_2\text{-CeO}_2$  (in air) excluding the tetragonal  $\rightarrow$  cubic transition for  $\text{ZrO}_2$ -rich compositions. Reduction of the cerium oxide component at subsolidus and liquidus temperatures also is not suggested. This diagram provides a more reliable liquidus with a minimum suggested near 60 mol% cerium oxide and  $\approx 2310^\circ$ . The approximate  $\text{Ce}^{3+}$  content at the liquidus temperature  $[\text{Ce}^{3+}/(\text{Ce}^{3+} + \text{Ce}^{4+}) (\%) ]$  (shown on top of diagram) was recalculated from graphical data presented. Note that reduction is extensive from cerium oxide ( $\text{CeO}_{1.85}$ ,  $2445^\circ$ ) to a maximum near 70 mol%  $\text{ZrO}_2$ . Liquidus temperatures for compositions having  $<25$  mol%  $\text{ZrO}_2$  are subjected to greater error because of the vaporization of the cerium oxide component. X-ray data for quenched but recrystallized liquids and for reoxidized materials are given.

1. A. Rouanet, Thesis, University of Montpellier, 1970; 109 pp.
2. M. Foex, *Rev. Int. Hautes Temp. Refract.*, **3** [3] 309 (1966). T.N.

## Co-Li-O

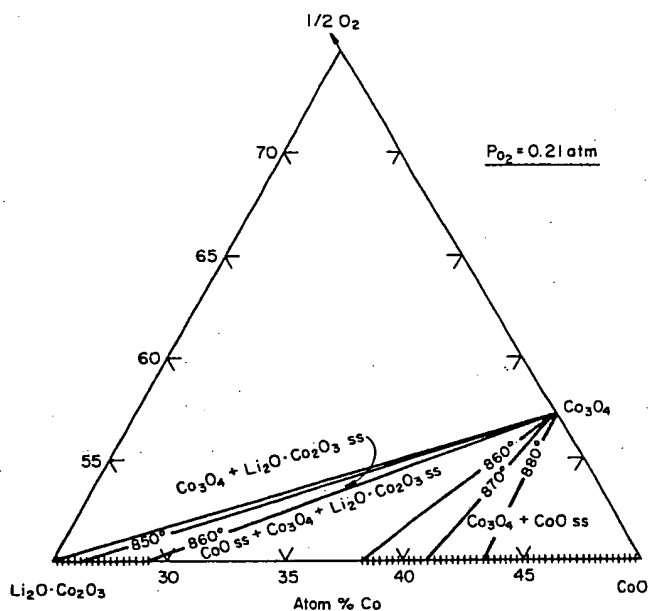


FIG. 5043.—System  $\text{Li-Co-O}$ .  
R. J. Moore and J. White, *J. Mater. Sci.*, **9** [9] 1401 (1974).

The starting materials appear to have been of ordinary reagent grade purity, although precise details are not supplied. Equilibrium relationships were established in air using a thermobalance. Prefired pellets were prepared by heating  $\text{Li}_2\text{CO}_3\text{-Co}_3\text{O}_4$  mixtures in air at  $800^\circ$  for 3 h. The compositions of the pellets were determined by quantitative flame-photometric analysis for Li. The pellets were first equilibrated on the thermobalance at  $930^\circ$  and brought into equilibrium at progressively lower temperatures. Although much Li loss occurred during the initial firing, Li loss was negligible during the actual equilibrations on the thermobalance. Five compositions were studied at closely spaced temperatures between  $800^\circ$  and  $\approx 950^\circ$ ; an isobaric phase diagram was constructed from the weight changes. Up to  $860^\circ$ , mixtures in equilibrium with air consisted of a two-phase assemblage ( $\text{Co}_3\text{O}_4$  and  $\text{LiCoO}_2$  ss) but, at  $860^\circ$ , they enter the three-phase triangle ( $\text{LiCoO}_2$  ss +  $\text{Co}_3\text{O}_4$  +  $\text{CoO}$  ss) while above this temperature the stable assemblage is ( $\text{CoO}$  ss +  $\text{Co}_3\text{O}_4$ ). This interpretation was confirmed by microscopic examination of polished sections. The diagram shows the position of the two-phase tie lines at  $850^\circ$ ,  $870^\circ$ , and  $880^\circ$  as well as the three-phase assemblage at  $860^\circ$ . Limits of solid solution on the  $\text{Li}_2\text{O}\cdot\text{Co}_2\text{O}_3\text{-CoO}$  join are shown by cross-hatching. F.P.G.

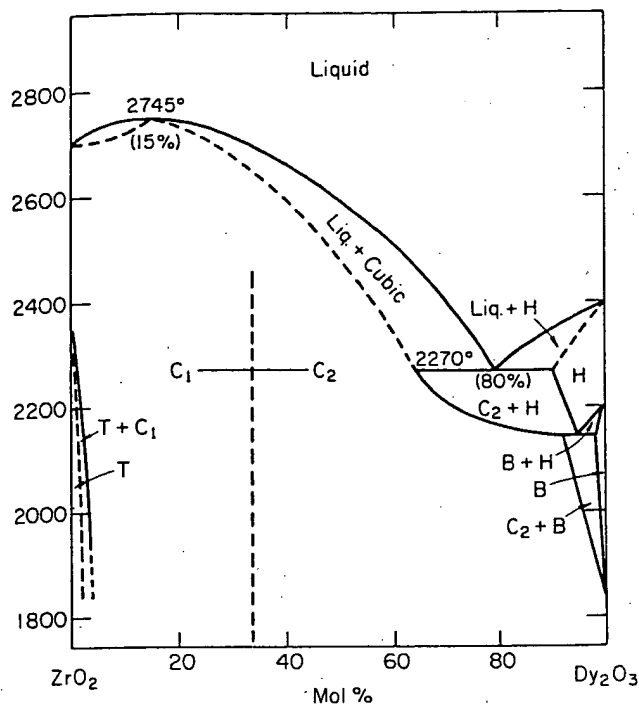
**Dy<sub>2</sub>O<sub>3</sub>-ZrO<sub>2</sub>**

FIG. 5211.—System ZrO<sub>2</sub>-Dy<sub>2</sub>O<sub>3</sub>. B = monoclinic phase, C<sub>1</sub> = cubic ss of the CaF<sub>2</sub> type, C<sub>2</sub> = cubic ss of the Ti<sub>2</sub>O<sub>3</sub> type, H = hexagonal ss, T = tetragonal ss having narrow limits of existence near compounds.

A. Rouanet, *Rev. Int. Hautes Temp. Refract.*, 8 [2] 161 (1971).

Liquidus curves and phase transformations in the solid state were obtained with the methods described in Fig. 5232. All dashed curves are estimated. ZrO<sub>2</sub> (99.9% without HfO<sub>2</sub>) and Dy<sub>2</sub>O<sub>3</sub> (99.9%) were the starting materials. For the polymorphism of ZrO<sub>2</sub> and Dy<sub>2</sub>O<sub>3</sub> see Fig. 4259 and Ref. 1, respectively. In the zirconia-rich side, the T → C<sub>1</sub> transition is reversible. Above 2000°, solid solutions vary from a cubic fluorite structure (C<sub>1</sub>, ZrO<sub>2</sub>-rich side) to a cubic Ti<sub>2</sub>O<sub>3</sub>-type structure (C<sub>2</sub>, Dy<sub>2</sub>O<sub>3</sub>-rich side). The author states that the C<sub>1</sub> → C<sub>2</sub> transition is continuous with a theoretical boundary at the 2ZrO<sub>2</sub>:Dy<sub>2</sub>O<sub>3</sub> composition. The ordered compound of the M<sub>7</sub>O<sub>11</sub> type, reported by Perez y Jorba,<sup>2</sup> was not found. On the Dy<sub>2</sub>O<sub>3</sub>-rich side, the H phase shows a eutectoid decomposition at 2150° giving C<sub>2</sub> + B (composition of the eutectoid, 5%ZrO<sub>2</sub>-95%Dy<sub>2</sub>O<sub>3</sub>). To better define this system (especially the C<sub>1</sub> → C<sub>2</sub> transition), additional studies involving long term equilibration in the 1800° to 2200° range appear necessary.

1. M. Foex, *Rev. Int. Hautes Temp. Refract.*, 3 [3] 309 (1966).

2. M. Perez y Jorba, *Ann. Chim. (Paris)*, 7 [7-8] 479 (1962).

J.P.C.

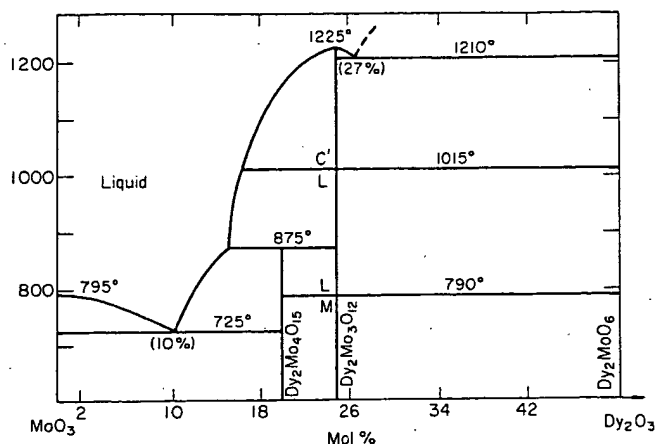
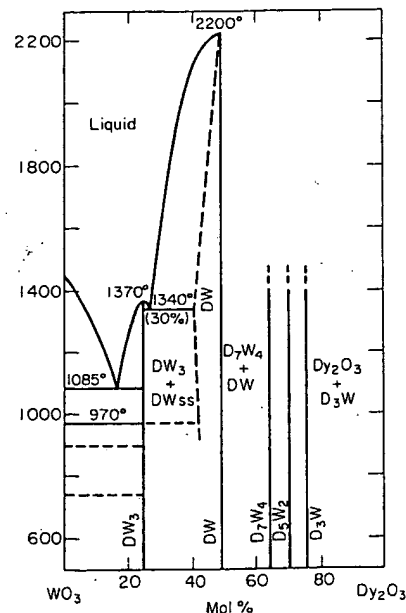
**Dy<sub>2</sub>O<sub>3</sub>-MoO<sub>3</sub>**

FIG. 5212.—System MoO<sub>3</sub>-Dy<sub>2</sub>O<sub>3</sub>.

G. V. Lysanova, L. Z. Gokhman, and N. G. Evdokimova, *Izv. Akad. Nauk SSSR, Neorg. Mater.*, 7 [11] 2025 (1971); *Inorg. Mater. (Engl. Transl.)*, 7 [11] 1802 (1971).

Mixtures of the oxides were subjected to stagewise annealing with intermediate grindings. The initial annealing temperature was not more than 500° to avoid loss of MoO<sub>3</sub> by volatilization; the temperature was then raised gradually by 100° after every 10 to 20 h. The final annealing temperature for samples with 2 to 18 mol% Dy<sub>2</sub>O<sub>3</sub> was 630°; for 20 to 24 mol% Dy<sub>2</sub>O<sub>3</sub>, 700°; for 25 to 60 mol% Dy<sub>2</sub>O<sub>3</sub>, 1000° to 1100°; for 60 to 100 mol% Dy<sub>2</sub>O<sub>3</sub>, 1200°. The duration of annealing at the final temperature was 150 to 250 h. Samples after annealing were analyzed for MoO<sub>3</sub> content, but results are not given. Phase relations in the system were determined by DTA, X-ray diffractometry, and densimetric analysis.

Dy<sub>2</sub>Mo<sub>3</sub>O<sub>12</sub> exists in three forms (M, L, and C'). Rapid cooling to room temperature was required for the preparation of C' from either the mixture of starting oxides or M- and L-forms. Slow cooling produced the L-form (the L to M transition is extremely sluggish). The C'-form is hygroscopic. Unindexed X-ray diffraction data are given. L.L.Y.C.

**Dy<sub>2</sub>O<sub>3</sub>-WO<sub>3</sub>**

BEST AVAILABLE COPY

**Er<sub>2</sub>O<sub>3</sub>-TiO<sub>2</sub> (concl.)**

J. Leban, D. Kolar, and Lj. Golic, *Monatsh. Chem.*, **103** [4] 1044 (1972).

The pyrochlore compound,  $\text{Er}_2\text{Ti}_2\text{O}_7$ , exists as a solid solution from 33.3 mol%  $\text{Er}_2\text{O}_3$  to  $\approx 50$  mol%  $\text{Er}_2\text{O}_3$  where it transforms into a fluorite-type (disordered) solid solution. The upper limit of the fluorite solution is  $\approx 57$  mol%  $\text{Er}_2\text{O}_3$  at  $1550^\circ$  and shifts slightly with temperature. X-ray data are given for various compositions of the pyrochlore and fluorite phases.

Below 1600°, virtually no  $\text{TiO}_2$  is soluble in the C-type  $\text{Er}_2\text{O}_3$  phase. M.F.B.

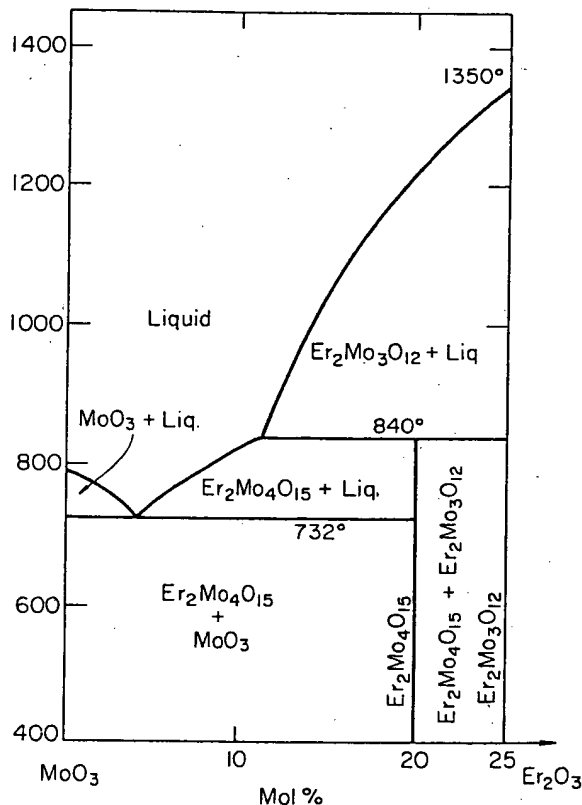
1. M. Foex and J. P. Traverse, *Rev. Int. Hautes Temp. Refract.*, 3 [3] 309 (1966).

2. J. P. Coutures, R. Verges, and M. Foex, *ibid.*, **12** [2] 181 (1975).

3. F. M. Spiridonov and L. N. Komissarova, *Zh. Neorg. Khim.*, **15** [3] 875 (1970); *Russ. J. Inorg. Chem. (Engl. Transl.)*, **15** [3] 445 (1970).

4. M. Perez y Jorba, *Ann. Chim. (Paris)*, 7 [7-8] 479 (1962).

J.P.C.

$$\text{Er}_2\text{O}_3\text{-MoO}_3$$


A. Rouanet, *Rev. Int. Hautes Temp. Refract.*, **8** [2] 161 (1971); P. Duran, *J. Am. Ceram. Soc.*, **60** [11-12] 510 (1977).

For the zirconia-rich side, a detailed study of the monoclinic (M), tetragonal (T), and cubic (C<sub>1</sub>) relations is given by Duran. The melting point of Er<sub>2</sub>O<sub>3</sub> is taken from Ref. 2. At high temperature (>2000°), solid solutions vary from a cubic fluorite structure (C<sub>2</sub>) to a cubic Ti<sub>2</sub>O<sub>3</sub>-type structure (C<sub>1</sub>). Rouanet states that the C<sub>1</sub> → C<sub>2</sub> transition is continuous with a theoretical boundary at the 2ZrO<sub>2</sub>·Er<sub>2</sub>O<sub>3</sub> composition. By long time annealing and quenching, Duran found new phases in the 1000° to 2000° range. In the 25% to 45% Er<sub>2</sub>O<sub>3</sub> range, an ordered, hexagonal phase of the M<sub>7</sub>O<sub>12</sub> type

FIG. 5218.—System  $\text{MoO}_3\text{--Er}_2\text{O}_3$ .  
S. S. Antonova, I. V. Shakno, and V. E. Plyushchev, *Izv. Vyssh. Uchebn. Zaved., Khim. Khim. Tekhnol.*, **14** [1] 17 (1971).

Samples were prepared by prolonged heating and slow cooling of oxide mixtures in air at 500° to 650°. Analysis was carried out by DTA and X-ray diffractometry. Unit cell parameters of the incongruently melting compound  $\text{Er}_2\text{Mo}_4\text{O}_{15}$  (1:4) are given. The system is qualitatively similar to the systems  $\text{MoO}_3\text{-Y}_2\text{O}_3$  and  $\text{MoO}_3\text{-Sm}_2\text{O}_3$ , described in the same reference (Figs. 5254 and 5246).

## BEST AVAILABLE COPY

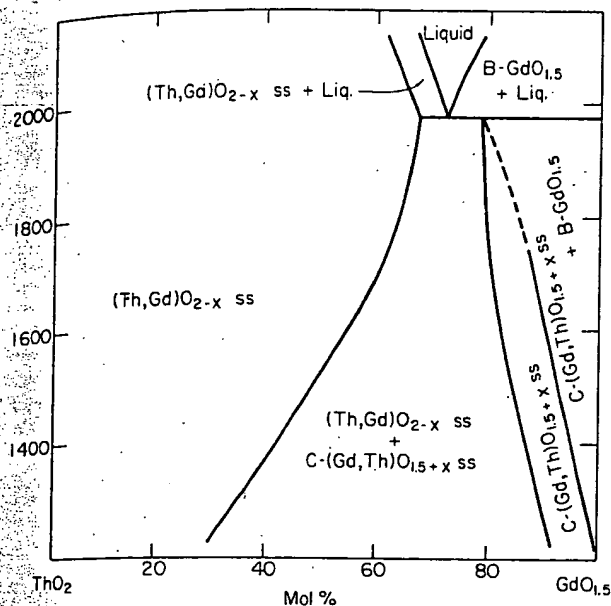
 $Gd_2O_3$ - $ThO_2$ 

FIG. 5222.—System  $ThO_2$ - $Gd_2O_3$ .  
C. Keller, U. Berndt, H. Engerer, and L. Leitner, *J. Solid State Chem.*, 4 [3] 453 (1972).

Coprecipitation of hydroxides was compared to direct mixing. Evaluation of the approach to equilibrium indicated coprecipitation to be superior and this method was used in sample preparation. High temperature X-ray phase analysis and room temperature quenches were compared, and the results indicated that room temperature quenches were accurately representative of the high temperature patterns. Thus, quenched samples were used for phase determinations. The temperature range considered was 1250° to 2100°. Based on density measurements, the anion vacancy model is verified for thorium-lanthanum systems.

The coincidence (in temperature) of eutectic (?) melting with  $(Gd,Th)O_{1.5+x}$  ss decomposition is not allowed by the phase rule; perhaps peritectic and eutectic melting occur at closely spaced intervals. See also Figs. 4415 and 5223. D.R.W.

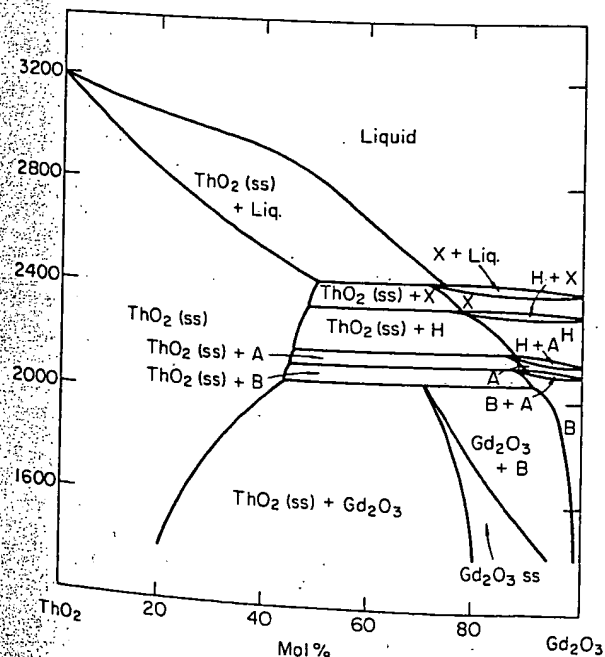


FIG. 5223.—System  $ThO_2$ - $Gd_2O_3$ . B = monoclinic (ss), A, H = hexagonal (ss), X = cubic (ss).

F. Sibieude and M. Foex, *J. Nucl. Mater.*, 56 [2] 229 (1975).

The liquidus curve and phase transformations in the solid state were obtained by methods described in Fig. 5231. The liquidus and solidus curves between  $ThO_2$  and 50% $ThO_2$ -50% $Gd_2O_3$  are estimated.

This diagram is tentative and based on experimental results obtained by thermal analysis and high temperature X-ray diffraction and data for the polymorphism of  $Gd_2O_3$ .<sup>1</sup>

The liquidus curve is characterized by a peritectic found on the  $Gd_2O_3$ -rich side ( $\approx 18\%ThO_2$ -82% $Gd_2O_3$ ) at 2400°.

In contrast to the  $ThO_2$ - $La_2O_3$ ,  $ThO_2$ - $Nd_2O_3$ , and  $ThO_2$ - $Sm_2O_3$  systems, no ordered phases were found, and the solution of  $Gd_2O_3$  in cubic  $ThO_2$  increases rapidly with temperature. The C, B, A, H, and X phases of  $Gd_2O_3$  show peritectoid decomposition. This diagram is in good agreement with Fig. 4415.

1. M. Foex and J. P. Traverse, *Rev. Int. Hautes Temp. Refract.*, 3 [4] 429 (1966). J.P.C.

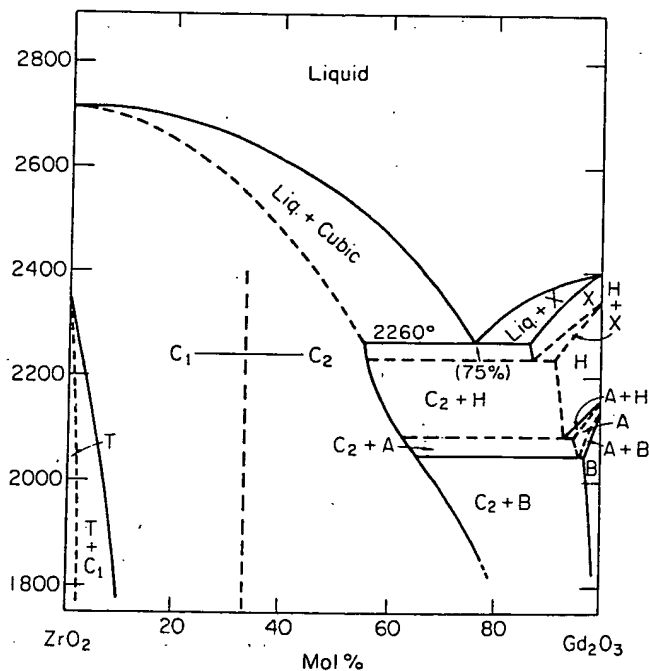
 $Gd_2O_3$ - $ZrO_2$ 

FIG. 5224.—System  $ZrO_2$ - $Gd_2O_3$ .

A. Rouanet, *Rev. Int. Hautes Temp. Refract.*, 8 [2] 161 (1971).

Liquidus curves and phase transitions in the solid state were obtained by methods described in Fig. 5232. All dashed curves are estimated.  $ZrO_2$  (99.9% without  $HfO_2$ ) and  $Gd_2O_3$  (99.9%) were the starting materials. See Fig. 4259 and Ref. 1 for the polymorphism of  $ZrO_2$  and  $Gd_2O_3$ , respectively.

For the  $Gd_2O_3$ -rich portion, this work differs significantly from Fig. 2369, which was constructed using coprecipitated materials, followed by annealing at various temperatures, in some cases over 2000°. One of the major differences is the stability of a hexagonal (H), ordered phase. The X phase could not be quenched and was difficult to study at high temperature (to near the melting point) due to preferential vaporization of  $Gd_2O_3$ . Therefore, its homogeneity range could not be determined. The original diagram shows a

**Gd<sub>2</sub>O<sub>3</sub>-ZrO<sub>2</sub> (concl.)**

peritectic point near 10%ZrO<sub>2</sub>-90%Gd<sub>2</sub>O<sub>3</sub> but this is questionable based on data in Ref. 1. This region is redrawn to include a limited stability range for a biphasic region, C<sub>2</sub> + X. The hexagonal (H) form in the original diagram has a eutectoid decomposition at 2050° (10%ZrO<sub>2</sub>-90%Gd<sub>2</sub>O<sub>3</sub>) giving C<sub>2</sub> + B. However, because of the Gd<sub>2</sub>O<sub>3</sub> polymorphism, the moderate temperature range of the Gd<sub>2</sub>O<sub>3</sub>-rich side also is redrawn (see commentary for Fig. 5245).

On the zirconium-rich side, this diagram differs from Fig. 2370. As shown in Fig. 2369, however, an ordered pyrochlore compound (Gd<sub>2</sub>Zr<sub>2</sub>O<sub>7</sub>) is stable but disorders above ≈1550° which is below the temperature range of this study. The tetragonal (T) → C<sub>1</sub> transition is reversible. The author states that the C<sub>1</sub> → C<sub>2</sub> (cubic fluorite → cubic Ti<sub>2</sub>O<sub>3</sub>) transition appears to be continuous with a theoretical boundary at the pyrochlore composition.

This diagram appears to be the best available. However the C<sub>1</sub> → C<sub>2</sub> transition (a biphasic region must exist) and the Gd<sub>2</sub>O<sub>3</sub>-rich side could be better defined.

1. M. Foex and J. P. Traverse, *Rev. Int. Hautes Temp. Refract.*, 3 [4] 429 (1966). J.P.C.

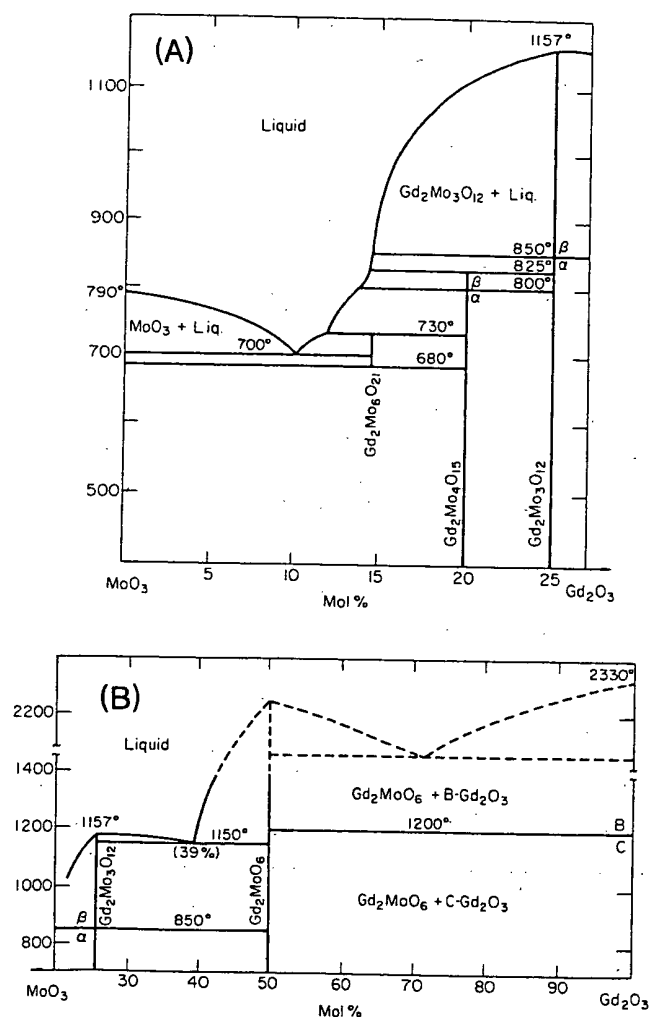
**Gd<sub>2</sub>O<sub>3</sub>-MoO<sub>3</sub>**

FIG. 5225.—System MoO<sub>3</sub>-Gd<sub>2</sub>O<sub>3</sub>. (A) MoO<sub>3</sub>-rich portion and (B) region between 25 and 100 mol% Gd<sub>2</sub>O<sub>3</sub>.

K. Megumi, H. Yumoto, S. Ashida, S. Akiyama, and Y. Furuhashi, *Mater. Res. Bull.*, 9 [4] 391 (1974).

**BEST AVAILABLE COPY**

Gd<sub>2</sub>O<sub>3</sub> and MoO<sub>3</sub> of specpure grade were used as starting materials. They were mixed for 5 h in dried air, pelletized, and sintered to prepare the samples. DTA and X-ray diffractometry were used for the determination of phase relations. Samples exhibiting multiple heat anomalies were measured more than twice by changing cycling rate and the quantity of the samples to reproduce the DTA curves.

In (A), two compounds were found. The composition of the MoO<sub>3</sub>-rich compound, although given as Gd<sub>2</sub>Mo<sub>6</sub>O<sub>21</sub>, is not well established based on experimental data presented. Two DTA maximums were observed for Gd<sub>2</sub>Mo<sub>4</sub>O<sub>15</sub> at 825° and 800°, illustrating a peritectic reaction and a phase transition, respectively. The phase transition was not confirmed by X-ray diffractometry.

In (B), only Gd<sub>2</sub>Mo<sub>3</sub>O<sub>12</sub> and Gd<sub>2</sub>MoO<sub>6</sub> were found to be stable phases. Attempts made to synthesize both Gd<sub>18</sub>Mo<sub>9</sub>O<sub>39</sub> and Gd<sub>6</sub>MoO<sub>12</sub> failed. Gd<sub>2</sub>Mo<sub>3</sub>O<sub>12</sub> is dimorphic with a transition temperature detected at 850°. The transition from α (low temperature) form to β (high temperature) form is instantaneous, whereas the reverse reaction is very sluggish. The reported γ form<sup>2</sup> was not found. Unindexed X-ray powder diffraction data are given.

1. F. P. Alekseev, E. I. Get'man, G. G. Koshcheev, and M. V. Mokhosoev, *Zh. Neorg. Khim.*, 14 [11] 2954 (1969); *Russ. J. Inorg. Chem. (Engl. Transl.)*, 14 [11] 1558 (1969).  
 2. K. Nassau, P. B. Jamieson, and J. W. Shiever, *J. Phys. Chem. Solids*, 30 [5] 1225 (1969). L.L.Y.C.

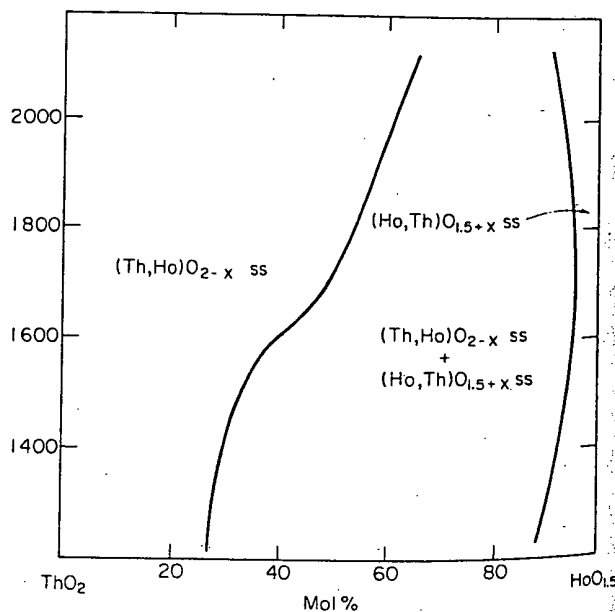
**Ho<sub>2</sub>O<sub>3</sub>-ThO<sub>2</sub>**

FIG. 5226.—System ThO<sub>2</sub>-Ho<sub>2</sub>O<sub>3</sub>. C. Keller, U. Berndt, H. Engerer, and L. Leitner, *J. Solid State Chem.*, 4 [3] 453 (1972).

Coprecipitation of hydroxides was compared to direct mixing. Evaluation of the approach to equilibrium indicated that coprecipitation was superior and this method was used in sample preparation. High temperature X-ray phase analysis and room temperature quenches were compared and the results indicated that room temperature quenches were accurately representative of the high temperature patterns. Thus, quenched samples were used for phase determinations. The temperature range considered was 1250° to 2100°. Based on density measurements, the anion vacancy model is verified for thorium-lanthanum systems. Compare with Fig. 5227. D.R.W.

# BEST AVAILABLE COPY

## Ho<sub>2</sub>O<sub>3</sub>-ThO<sub>2</sub> (concl.)

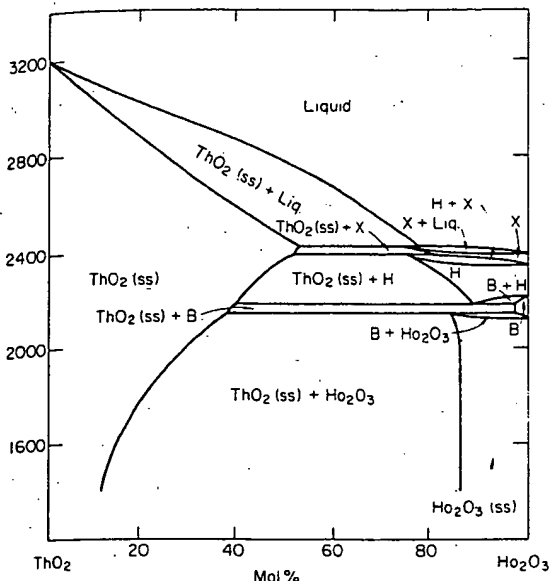


FIG. 5227.—System ThO<sub>2</sub>-Ho<sub>2</sub>O<sub>3</sub>. B = monoclinic (ss), H = hexagonal (ss), X = cubic (ss).  
F. Sibieude and M. Foex, *J. Nucl. Mater.*, 56 [2] 229 (1975).

The liquidus curve and phase transformations in the solid state were obtained by methods described in Fig. 5231. The liquidus and solidus curves between ThO<sub>2</sub> and 45%ThO<sub>2</sub>-55%Ho<sub>2</sub>O<sub>3</sub> are estimated.

This diagram is tentative and is based on experimental results obtained by thermal analysis and high temperature X-ray diffraction and data for the polymorphism of Ho<sub>2</sub>O<sub>3</sub>.<sup>1</sup> This diagram, except for the stability range of the B, H, and X forms of Ho<sub>2</sub>O<sub>3</sub>, is identical to that for the system ThO<sub>2</sub>-Dy<sub>2</sub>O<sub>3</sub>.

I. M. Foex and J. P. Traverse, *Rev. Int. Hautes Temp. Refract.*, 3 [4] 429 (1966). J.P.C.

## Ho<sub>2</sub>O<sub>3</sub>-ZrO<sub>2</sub>

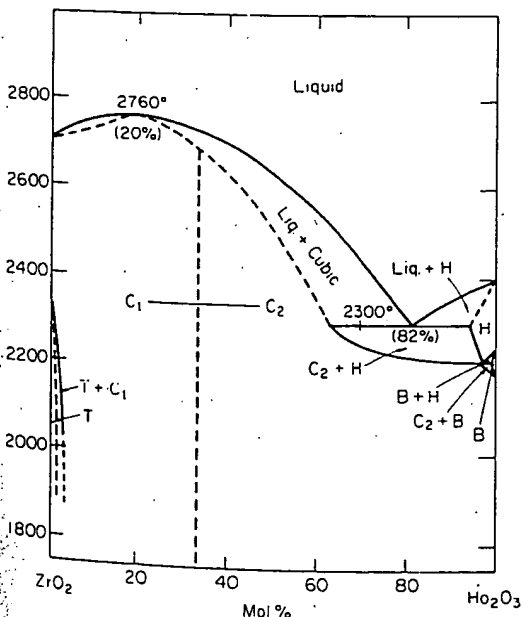


FIG. 5228.—System ZrO<sub>2</sub>-Ho<sub>2</sub>O<sub>3</sub>. B = monoclinic structure, C<sub>1</sub> = cubic ss of CaF<sub>2</sub> type, C<sub>2</sub> = cubic ss of Ti<sub>2</sub>O<sub>3</sub> type, H = hexagonal ss, T = tetragonal ss.

A. Rouanet, *Rev. Int. Hautes Temp. Refract.*, 8 [2] 161 (1971).

Liquidus curves and phase transformations in the solid state were obtained by methods described in Fig. 5232. All dashed curves are estimated. ZrO<sub>2</sub> (99.9% without HfO<sub>2</sub>) and Ho<sub>2</sub>O<sub>3</sub> (99.9%) were the starting materials. For the polymorphism of ZrO<sub>2</sub> and Ho<sub>2</sub>O<sub>3</sub>, see Fig. 4259 and Ref. 1, respectively. This diagram is similar to Fig. 5211 and similar comments are pertinent.

I. M. Foex and J. P. Traverse, *Rev. Int. Hautes Temp. Refract.*, 3 [4] 429 (1966). J.P.C.

## La<sub>2</sub>O<sub>3</sub>-GeO<sub>2</sub>

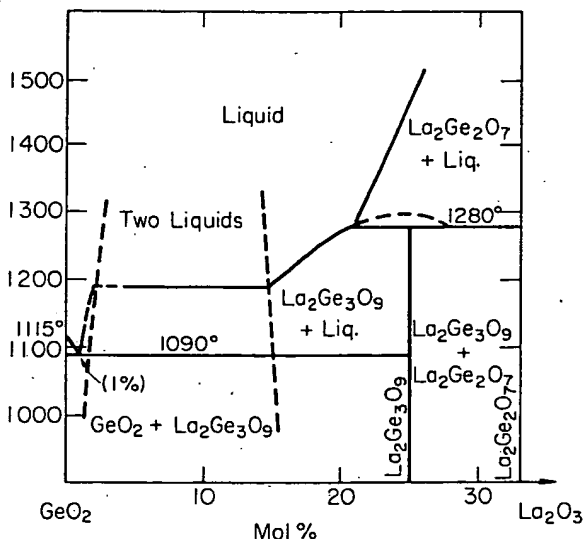


FIG. 5229.—System GeO<sub>2</sub>-La<sub>2</sub>O<sub>3</sub>.

N. G. Gutkina, I. I. Kozhina, and L. K. Shmatock, *Izv. Akad. Nauk SSSR, Neorg. Mater.*, 7 [8] 1382 (1971); *Inorg. Mater. (Engl. Transl.)*, 7 [8] 1228 (1971).

Synthesis was carried out in Pt crucibles using cp grade GeO<sub>2</sub> and La<sub>2</sub>O<sub>3</sub> with heating to 1500°-1640°. Analysis was accomplished by application of polythermal, optical, X-ray diffraction, and ir methods to quenched specimens that were annealed isothermally and in temperature gradients.

The diagram indicates the temperature at which flow of crystallized fragments occurred on heating and probably does not represent the true liquidus. It is said to be an approximate equilibrium diagram. A region of immiscibility was found in melts at high GeO<sub>2</sub> contents. La<sub>2</sub>Ge<sub>2</sub>O<sub>7</sub> melts congruently and forms a metastable eutectic with the incongruently melting La<sub>2</sub>Ge<sub>3</sub>O<sub>9</sub>. The latter phase forms a true eutectic with GeO<sub>2</sub> at 1090° and 1 mol% La<sub>2</sub>O<sub>3</sub>. Refractive index values of vitreous and crystalline phases are listed in a table.

M.F.B.

$\text{La}_2\text{O}_3\text{-ZrO}_2$ 

## BEST AVAILABLE COPY

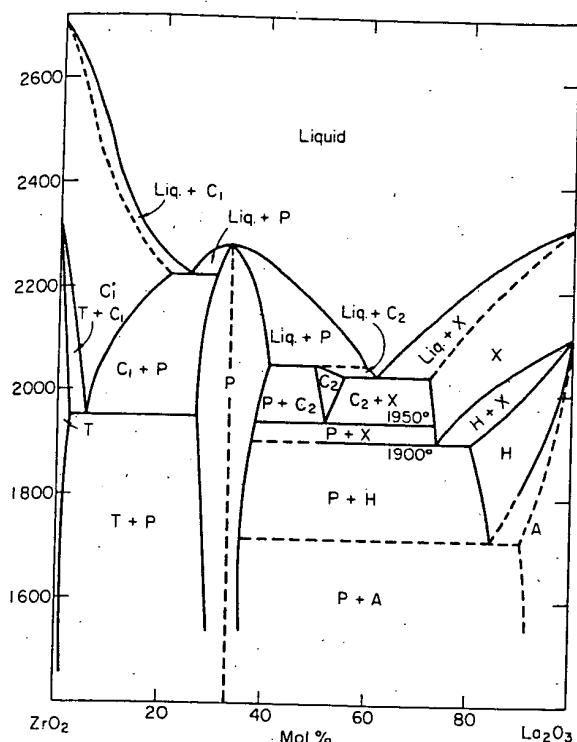


Fig. 5232. — System  $\text{ZrO}_2\text{-La}_2\text{O}_3$ . A = hexagonal ss,  $C_1$  = cubic ss of the  $\text{CaF}_2$  type,  $C_2$  = cubic ss of the  $\text{Ti}_2\text{O}_3$  type, H = hexagonal ss, P = pyrochlore-type compound, T = tetragonal ss, X = cubic ss. A. Rouanet, *Rev. Int. Hautes Temp. Refract.*, 8 [2] 161 (1971).

The liquidus curve was obtained from cooling curves obtained with a thermal analysis device associated with a 2 kW horizontal axis solar furnace.<sup>1</sup> Solidus curves (dashed lines) were estimated. To prevent contamination, runs were performed in air without crucibles. Temperatures were measured by optical pyrometry assuming an average emissivity of 0.5. The pyrometer ( $0.65\ \mu\text{m}$  with a Cs cell) was calibrated against the melting points of  $\text{ZrO}_2$  ( $2710^\circ$ ) and  $\text{Al}_2\text{O}_3$  ( $2050^\circ$ ). Phase transitions above  $1800^\circ$  were observed by high temperature X-ray diffraction using a Re ribbon under reducing conditions ( $\text{He} + \approx 10\% \text{H}_2$ ). These conditions could affect temperature measurements associated with phase transitions. Samples were pre-melted in air using solar furnaces, finely crushed, and deposited on the heating element.

The purity of the  $\text{ZrO}_2$  starting material was 99.9% (excluding  $\text{HfO}_2$ ) and that of the  $\text{La}_2\text{O}_3$  was 99.99%. The diagram shows a definite compound (pyrochlore phase type) with a congruent melting point ( $2280^\circ$ ) surrounded by two eutectics, 75% $\text{ZrO}_2$ -25% $\text{La}_2\text{O}_3$  ( $2220^\circ$ ) and 37.5% $\text{ZrO}_2$ -62.5% $\text{La}_2\text{O}_3$  ( $2030^\circ$ ). Cabannes *et al.*<sup>2</sup> measured the melting point of the first eutectic in air and in oxygen ( $2224^\circ \pm 10^\circ$ ). In argon, the reduction of  $\text{ZrO}_2$  decreases the melting point by  $45^\circ$ . For polymorphism of  $\text{ZrO}_2$  see Fig. 4259, and for  $\text{La}_2\text{O}_3$ , see Ref. 3.

The apparent inflection on the liquidus curve between  $\text{ZrO}_2$  and the  $\text{ZrO}_2\text{-La}_2\text{Zr}_2\text{O}_7$  eutectic remains unexplained but corresponds to the experimental data.

The X phase could not be quenched and was difficult to study at high temperature because of excessive vaporization of  $\text{La}_2\text{O}_3$  near  $2100^\circ$ . Consequently, its homogeneity range could not be determined accurately. At  $1900^\circ$ , the maximum solubility of  $\text{ZrO}_2$  is  $\approx 30\%$ . The  $X \rightarrow H$  transition was observed easily by thermal analysis up to 15% of  $\text{ZrO}_2$ . The  $H \rightarrow A$  transformation, observed sharply for pure  $\text{La}_2\text{O}_3$ , is not well defined for solid solutions. Nevertheless, the phase transition temperature decreases sharply as the  $\text{ZrO}_2$  concentration increases. The eutectoid reaction at  $1900^\circ$  was determined by high temperature X-ray diffraction.

Although the  $C_2$  phase ( $C_2$ : cubic-type  $\text{Ti}_2\text{O}_3$ ) doesn't exist at high temperature for  $\text{La}_2\text{O}_3$ , solution of  $\text{ZrO}_2$  can stabilize this structure. The stability range ( $T$  and composition) is very limited but observed by high temperature X-ray diffraction. This  $C_2$  phase shows a eutectoid transformation (eutectoid point 48% $\text{ZrO}_2$ -52% $\text{La}_2\text{O}_3$ ,  $1950^\circ$ ) giving P and X phases.

The cubic  $\text{La}_2\text{Zr}_2\text{O}_7$  compound is stable to the melting point. Thermal expansion was measured by high temperature X-ray diffraction.

On the zirconia-rich side, the  $C_1$  cubic phase shows a eutectoid transformation (eutectoid point 93% $\text{ZrO}_2$ -7% $\text{La}_2\text{O}_3$ ,  $1950^\circ$ ) giving T and P phases. The  $T \rightarrow C_1$  transition is reversible.

This diagram differs from previous, incomplete diagrams (Figs. 346, 2374, 2375). It should be considered the best available. Future work is necessary to determine the precise stability range of the  $C_2$  solid solution and to provide an explanation of the inflection on the liquidus curve between  $\text{ZrO}_2$  and the  $\text{ZrO}_2\text{-La}_2\text{Zr}_2\text{O}_7$  eutectic.

1. M. Foex, *Rev. Int. Hautes Temp. Refract.*, 3 [3] 309 (1966).
2. F. Cabannes, J. Simonato, M. Foex, and J. P. Coutures, *High Temp.-High Pressures*, 4 [5] 589 (1972).
3. M. Foex and J. P. Traverse, *Rev. Int. Hautes Temp. Refract.*, 3 [4] 429 (1966).

J.P.C.

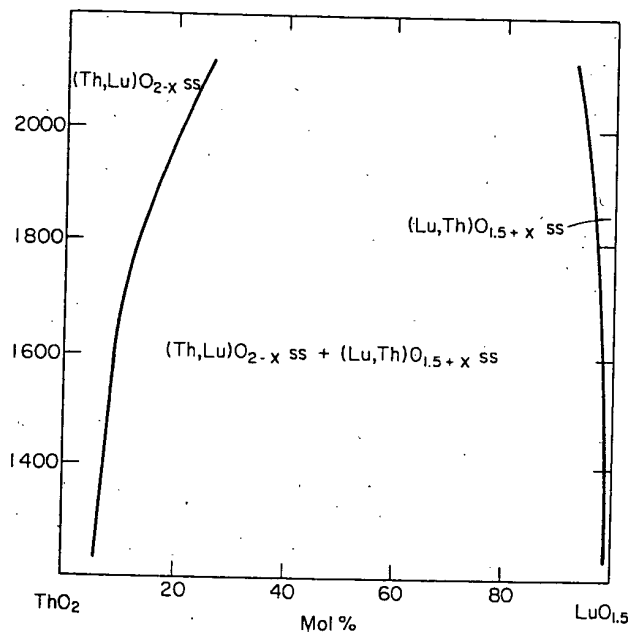
 $\text{Lu}_2\text{O}_3\text{-ThO}_2$ 

Fig. 5233. — System  $\text{ThO}_2\text{-Lu}_2\text{O}_3$ . C. Keller, U. Berndt, H. Engerer, and L. Leitner, *J. Solid State Chem.*, 4 [3] 453 (1972).

Coprecipitation of hydroxides was compared to direct mixing. Evaluation of the approach to equilibrium indicated that coprecipitation was superior and this method was used in sample preparation. High temperature X-ray phase analysis and room temperature quenches were accurately representative of the high temperature patterns. Thus, quenched samples were used for phase determinations. The temperature range considered was  $1250^\circ$  to  $2100^\circ$ . Based on density measurements, the anion vacancy model is verified for thorium-lanthanum systems.

D.R.W.



**Nd<sub>2</sub>O<sub>3</sub>-Yb<sub>2</sub>O<sub>3</sub> (concl.)**

The cubic C phase of Yb<sub>2</sub>O<sub>3</sub> dissolves up to ≈30 mol% Nd<sub>2</sub>O<sub>3</sub>. Premelted samples which were subsequently annealed at 1400° exhibited at room temperature a linear increase in lattice parameter with Nd<sub>2</sub>O<sub>3</sub> addition.

At normal pressures, there are no temperature ranges in which either Nd<sub>2</sub>O<sub>3</sub> or Yb<sub>2</sub>O<sub>3</sub> are stable in the monoclinic B form. However, when Yb<sub>2</sub>O<sub>3</sub> is added to Nd<sub>2</sub>O<sub>3</sub> in solid solution at lower temperatures, a B-type structure is formed (see Fig. 348). The compositional range of the B solid solutions is ≈3 to 40 mol% Yb<sub>2</sub>O<sub>3</sub>. For a discussion of the Nd<sub>2</sub>O<sub>3</sub>-rich, B structure solid solution, refer to Fig. 5234.

Pure Nd<sub>2</sub>O<sub>3</sub> has the hexagonal A structure at low temperatures and dissolves <1 mol% Yb<sub>2</sub>O<sub>3</sub> at 1400°. The solubility increases to a maximum of 35 to 40 mol% Yb<sub>2</sub>O<sub>3</sub> at 1940°. The A solid solutions transform to the hexagonal H form at higher temperatures. It is difficult to distinguish between the A and H forms by high-temperature X-ray diffraction. However, thermal arrests can be used to locate the apparent transformation temperatures for the A⇌H transformation.

The H polymorph of Nd<sub>2</sub>O<sub>3</sub> forms solid solutions extending nearly to Yb<sub>2</sub>O<sub>3</sub>. The temperature stability range for the H form shifts with composition. The presence of an H form for pure Yb<sub>2</sub>O<sub>3</sub> was not confirmed by X-ray diffraction, but a thermal effect (DTA) which may correspond to the C→H transformation was observed near the melting point of Yb<sub>2</sub>O<sub>3</sub>. Tresvyatskii *et al.*<sup>1</sup> also reported this effect. The addition of 1 to 2 mol% Nd<sub>2</sub>O<sub>3</sub> to Yb<sub>2</sub>O<sub>3</sub> readily forms the Y polymorph near the melting point.

The H form and X form (cubic) have not been retained at room temperature even by very rapid quenching. This may be due to the ready formation of the metastable and quite persistent B phase.

No compound (e.g. YbNdO<sub>3</sub>) was found. Refer to Fig. 5234 for a comparison with other Nd<sub>2</sub>O<sub>3</sub>-lanthanide systems.

I. S. G. Tresvyatskii, L. M. Lopato, A. V. Shevchenko, and A. E. Kushchewskii, *Colloq. Int. CNRS*, 1972, No. 205, p. 247.

M.F.B.

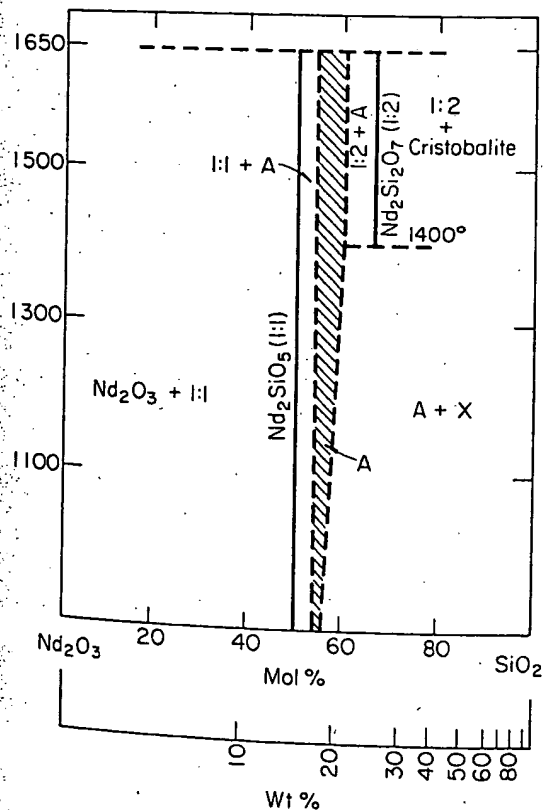
**Nd<sub>2</sub>O<sub>3</sub>-SiO<sub>2</sub>****BEST AVAILABLE COPY**

FIG. 5236.—System Nd<sub>2</sub>O<sub>3</sub>-SiO<sub>2</sub> in air.

N. A. Toporov and M. V. Kougiya, *Izv. Akad. Nauk SSSR, Neorg. Mater.*, 7 [7] 1220 (1971); *Inorg. Mater. (Engl. Transl.)*, 7 [7] 1082 (1971).

Specimens were synthesized by solid state reaction of mixtures of Nd<sub>2</sub>O<sub>3</sub> and SiO<sub>2</sub> in air at 1450° to 1650°. Optical, chemical, and X-ray diffraction analyses were used to identify phases.

The compound 1:1 (Nd<sub>2</sub>O<sub>3</sub>-SiO<sub>2</sub>) varied little in composition. The 1:2 compound also varies little in composition above 1400°. Below 1400°, the 1:2 compound decomposes into two phases, in agreement with Miller and Rose (Fig. 2380), who, however, show the decomposition at ≈1540°. The region marked A in the diagram represents one of these phases and corresponds to a composition of 7:9 below 1400° and to a composition of 2:3 (6:9)<sup>1</sup> above that temperature. There is a small solubility of Nd<sub>2</sub>O<sub>3</sub> in the A phase which has the apatite structure over the entire temperature range. The second phase, into which the 1:2 compound decomposes below 1400°, is designated the X phase and is a new phase not reported in Figs. 2380 and 2381. This phase is believed to be 1:3 or 1:4 in composition, but these compounds could not be synthesized by direct reaction of the end-member oxides.<sup>2</sup> A partial diffraction pattern is provided for the X phase, but no structural type is assigned.

1. G. J. McCarthy, W. B. White, and R. Roy, *J. Inorg. Nucl. Chem.*, 29 [1] 253 (1967).
2. A. N. Lazarev, *Covalent Spectra and the Structure of Silicates*, Nauka, Leningrad (1969).

M.F.B.

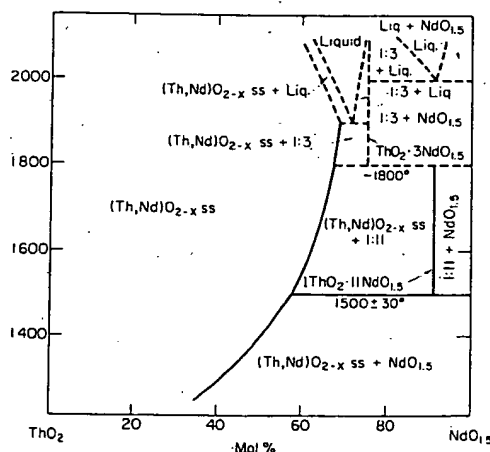
**Nd<sub>2</sub>O<sub>3</sub>-ThO<sub>2</sub>**

FIG. 5237.—System ThO<sub>2</sub>-NdO<sub>1.5</sub>.

C. Keller, U. Berndt, H. Engerer, and L. Leitner, *J. Solid State Chem.*, 4 [3] 453 (1972).

Coprecipitation of hydroxides was compared to direct mixing. Evaluation of the approach to equilibrium indicated that coprecipitation was superior and this method was used in sample preparation. High temperature X-ray phase analysis and room temperature quenches were compared and the results indicated that room temperature quenches were accurately representative of the high temperature patterns. Thus, quenched samples were used for phase determinations. The temperature range considered was 1250° to 2100°. Based on density measurements, the anion vacancy model is verified for thorium-lanthanum systems.

The coincidence (in temperature) of maximum and minimum decomposition of the 1:11 and 1:3 phases is not allowed by the phase rule; perhaps these two reactions occur at closely spaced temperatures. Compare with Fig. 5238.

D.R.W.

# $\text{Nd}_2\text{O}_3\text{-ThO}_2$ (concl.) **BEST AVAILABLE COPY** $\text{Nd}_2\text{O}_3\text{-ZrO}_2$

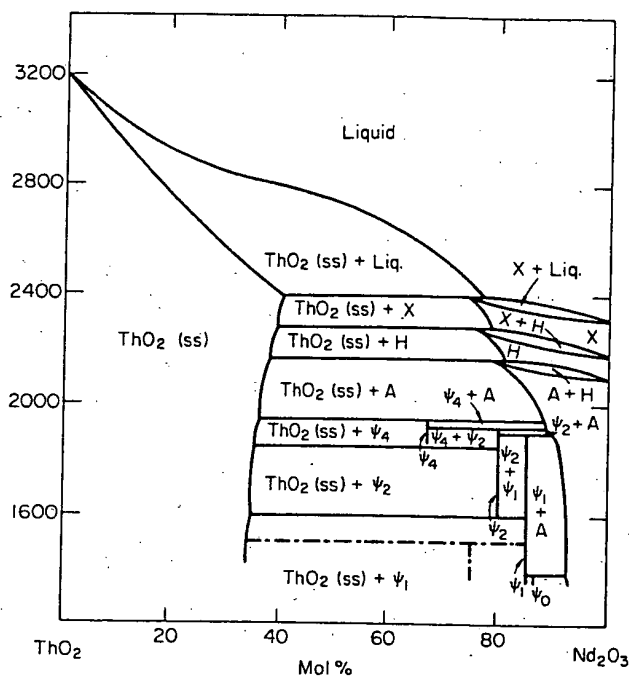


FIG. 5238.—System  $\text{ThO}_2\text{-Nd}_2\text{O}_3$ . A, H = hexagonal (ss), X = cubic (ss),  $\psi_0\text{-}\psi_4$  = hexagonal compounds. F. Sibieude and M. Foex, *J. Nucl. Mater.*, 56 [2] 229 (1975).

The liquidus curve and phase transformations in the solid state were obtained by methods described in Fig. 5231. The solidus curve is estimated.

This tentative phase diagram is based on using experimental results obtained by thermal analysis and high temperature X-ray diffraction and the polymorphism of  $\text{Nd}_2\text{O}_3$ .<sup>1</sup>

The liquidus did not show any compound with a congruent melting point, but an inflection near  $\text{ThO}_2$  ( $\approx 70\%\text{ThO}_2\text{-}30\%\text{Nd}_2\text{O}_3$ ) was found as well as a peritectic point on the  $\text{Nd}_2\text{O}_3$ -rich side ( $\approx 25\%\text{ThO}_2\text{-}75\%\text{Nd}_2\text{O}_3$ ) at  $2400^\circ$ . The high volatility of  $\text{Nd}_2\text{O}_3$  near  $2100^\circ$  made difficult the measurement of the  $\text{ThO}_2$  solubility in the H and X forms of  $\text{Nd}_2\text{O}_3$ . Nevertheless, it is obvious that the solubility in  $\text{Nd}_2\text{O}_3$  increases above  $2000^\circ$  to  $\approx 25\%\text{ThO}_2$  near the fusion point. The A, H, and X phases show a peritectoid decomposition with increasing temperature.

New ordered phases designated  $\psi_0$ ,  $\psi_1$ ,  $\psi_2$ ,  $\psi_3$ , and  $\psi_4$  were found. Phases  $\psi_1$  and  $\psi_2$  were obtained after quenching and were not decomposed by prolonged annealing at  $1400^\circ$ . Phases  $\psi_0$  and  $\psi_3$  were also obtained by quenching but decompose after annealing at  $1400^\circ$  giving, respectively,  $\psi_1 + \text{A}$   $\text{Nd}_2\text{O}_3$ ,  $\psi_2 + \text{ThO}_2$ . The  $\psi_4$  phase appears between  $1850^\circ$  and  $1950^\circ$ . The composition of the  $\psi_0$ ,  $\psi_1$ ,  $\psi_2$ ,  $\psi_3$ , and  $\psi_4$  phases is identical to  $\psi_0$ ,  $\psi_1$ ,  $\psi_2$ ,  $\psi_3$ , and  $\psi_4$  phases observed in the system  $\text{ThO}_2\text{-La}_2\text{O}_3$  (Fig. 5231). The  $\psi_3$  and  $\psi_4$  phases appear to be identical in the  $\text{ThO}_2\text{-La}_2\text{O}_3$  and  $\text{ThO}_2\text{-Nd}_2\text{O}_3$  diagrams.<sup>2</sup>

This diagram must be considered the best available for the same reasons mentioned in Fig. 5231, but new studies on the  $\text{Nd}_2\text{O}_3$ -rich side with high resolution electron microscopy would be desirable for a better understanding of the  $\psi_0$ ,  $\psi_1$ ,  $\psi_2$ ,  $\psi_3$ , and  $\psi_4$  relations.

1. M. Foex and J. P. Traverse, *Rev. Int. Hautes Temp. Refract.*, 3 [4] 429 (1966).

2. F. Sibieude, *J. Solid State Chem.*, 7 [1] 7 (1973).

J.P.C.

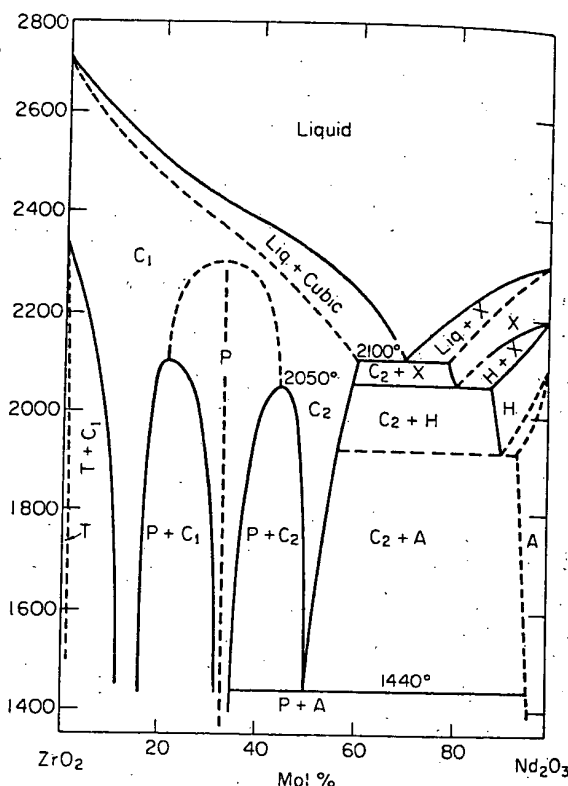


FIG. 5239.—System  $\text{ZrO}_2\text{-Nd}_2\text{O}_3$ . A = hexagonal ss,  $C_1$  = cubic ss of the fluorite type,  $C_2$  = cubic ss of the  $\text{Ti}_2\text{O}_3$  type, H = hexagonal ss, P = pyrochlore-type compound, T = tetragonal ss, X = cubic ss.

A. Rouanet, *Rev. Int. Hautes Temp. Refract.*, 8 [2] 161 (1971).

The liquidus curve was obtained from cooling curves obtained with a thermal analysis device associated with a 2 kW horizontal axis solar furnace.<sup>1</sup> The solidus curves (dashed lines) were estimated. To prevent contamination, runs were performed in air without crucibles. Temperatures were measured by optical pyrometry using an average emissivity of 0.5. The pyrometer was calibrated against the melting points of  $\text{ZrO}_2$  ( $2710^\circ$ ) and  $\text{Al}_2\text{O}_3$  ( $2050^\circ$ ). Phase transitions above  $1800^\circ$  were observed by high temperature X-ray diffraction using a Re ribbon under reducing conditions ( $\text{He} + \approx 10\%\text{H}_2$ ). These conditions could alter the temperatures associated with phase transitions. Samples were premelted in air using solar furnaces, finely crushed, and deposited on the heating element.

The purity of  $\text{ZrO}_2$  and  $\text{Nd}_2\text{O}_3$  used as starting materials was 99.9%. In the diagram the apparent inflection on the liquidus curve (at the pyrochlore, P, composition) could be due to a partial ordering of the liquid in this composition range. The melting point and composition of the eutectic between  $\text{ZrO}_2$  and  $\text{Nd}_2\text{O}_3$  are, respectively,  $2100^\circ$  and  $30\%\text{ZrO}_2\text{-}70\%\text{Nd}_2\text{O}_3$ .

The X phase could not be quenched and was difficult to study at high temperature because of the high volatility of  $\text{Nd}_2\text{O}_3$  near  $2100^\circ$ . Therefore, its stability range could not be determined accurately although the  $X \rightarrow H$  transition temperature decreases with increasing  $\text{ZrO}_2$  content. The  $H \rightarrow A$  transformation, easily observed for pure  $\text{Nd}_2\text{O}_3$ , is not clearly defined for solid solutions. At  $2060^\circ$ , the X phase shows a eutectoid decomposition giving  $C_2$  and H (X composition,  $20\%\text{ZrO}_2\text{-}80\%\text{Nd}_2\text{O}_3$ ;  $C_2$  composition,  $41\%\text{ZrO}_2\text{-}59\%\text{Nd}_2\text{O}_3$ ; H composition,  $13\%\text{ZrO}_2\text{-}87\%\text{Nd}_2\text{O}_3$ ). The eutectoid decomposition of  $C_2$  at  $1440^\circ$  yields P and A ( $C_2$  composition,  $50\%\text{ZrO}_2\text{-}50\%\text{Nd}_2\text{O}_3$ ; P composition,  $65\%\text{ZrO}_2\text{-}35\%\text{Nd}_2\text{O}_3$ ; A composition,  $5\%\text{ZrO}_2\text{-}95\%\text{Nd}_2\text{O}_3$ ).

BEST AVAILABLE COPY

**Nd<sub>2</sub>O<sub>3</sub>-ZrO<sub>2</sub> (concl.)**

The compound  $\text{Nd}_2\text{Zr}_2\text{O}_7$  does not retain its ordered structure to the melting point. The associated dashed line gives an estimated stability range for the ordered form assuming disorder above  $2300^\circ$  at the  $\text{Nd}_2\text{Zr}_2\text{O}_7$  composition. At this composition, the cooling curve<sup>1</sup> shows a thermal arrest at  $2250^\circ$ . This may reflect the order-disorder transition. At temperatures lower than  $2100^\circ$ , the solubility of  $\text{ZrO}_2$  and  $\text{Nd}_2\text{O}_3$  in  $\text{Nd}_2\text{Zr}_2\text{O}_7$  decreases giving two exsolution fields ( $P + C_1$  and  $P + C_2$ ).

In the zirconia-rich region the  $C_1$  phase is completely stabilized with an addition of 15 mol%  $Nd_2O_3$ . The  $T \rightarrow C_1$  transition is reversible. This diagram differs in detail from previous, incomplete diagrams (Figs. 350, 2382, 2383) but resembles most closely Fig. 2382. It should be considered the best diagram available. Future work should be performed to better define the immiscibility gaps and the  $C_1 \rightarrow P \rightarrow C_2$  transitions.

J. A. Rouanet, Thesis, 1970 reg. CNRS: A.O. 4239.

J.P.C.

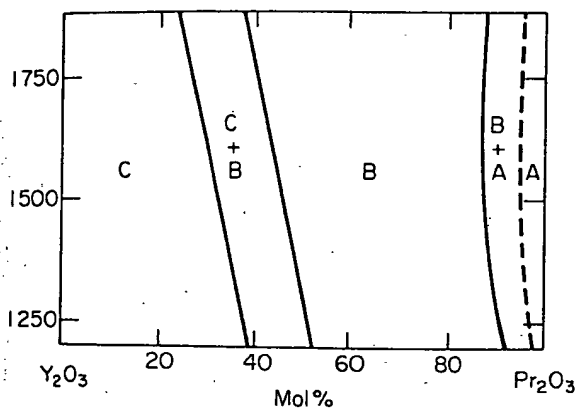
$$\text{Pr}_2\text{O}_3\text{-Y}_2\text{O}_3$$


FIG. 5240.—System  $Y_2O_3$ – $Pr_2O_3$ . C = cubic phase, B = monoclinic phase, A = hexagonal phase.

P. A. Tikhonov, K. Yu. Merezhinskii, and A. K. Kuznetsov, *Dokl. Akad. Nauk SSSR*, 222 [6] 1387 (1975); *Dokl. Phys. Chem. (Engl. Transl.)*, 222 [6] 650 (1975).

The starting materials consisted of 99.9%  $Y_2O_3$  and 99.8%  $Pr_6O_{11}$ . The oxides were mixed, pelletized, and heated at 1750° for 3 h in vacuum ( $10^{-1}$  mm Hg). Specimens were then heat-treated at 1250° (10 h), 1500° (5 h), and 1800° (2 h) in a vacuum of  $10^{-3}$  mm Hg, followed by quenching. Phases present were identified by X-ray diffraction.

Broad bands of solid solutions were found corresponding to the standard C and B forms of the rare earth oxide structures.<sup>1</sup> A narrow range of A-type solid solutions was found at high  $\text{Pr}_2\text{O}_3$  contents. Within the C and B structural types, the unit cell volume increased linearly with increasing mol%  $\text{Pr}_2\text{O}_3$ . The volume of the A unit cell also increased with increasing  $\text{Pr}_2\text{O}_3$  content, but only two points were determined.

The authors speculate that, while B forms for all rare earth oxides except  $Y_2O_3$  have been found at high pressures,<sup>2,3</sup> linear extrapolation of the B lattice parameters for  $Y_2O_3$ - $Pr_2O_3$  solid solutions to 0%  $Pr_2O_3$  is a valid method for estimating the lattice parameters for the as yet undiscovered B form of  $Y_2O_3$ .

1. J. D. McCullough and J. D. Britton, *J. Am. Chem. Soc.*, **74** [20] 5225 (1952).
2. H. R. Hoekstra and K. A. Gingerich, *Science*, **146** [3648] 1163 (1964).
3. H. R. Hoekstra, *Inorg. Chem.*, **5** [5] 754 (1966).

M.F.B:

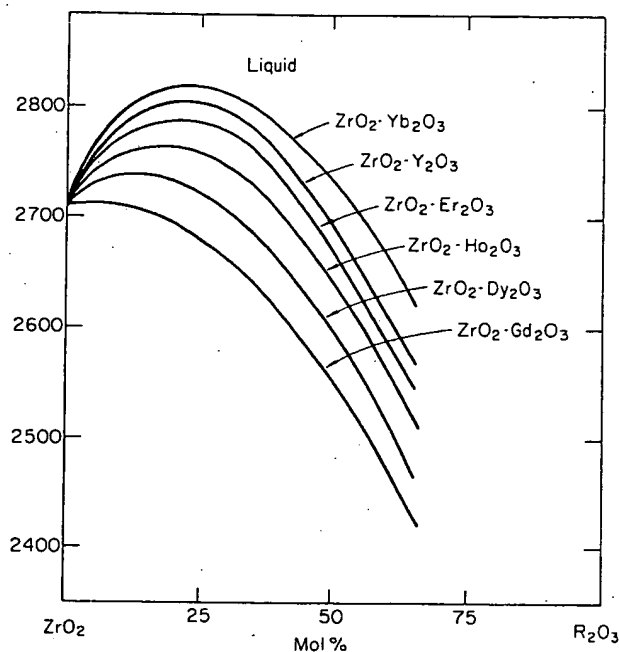
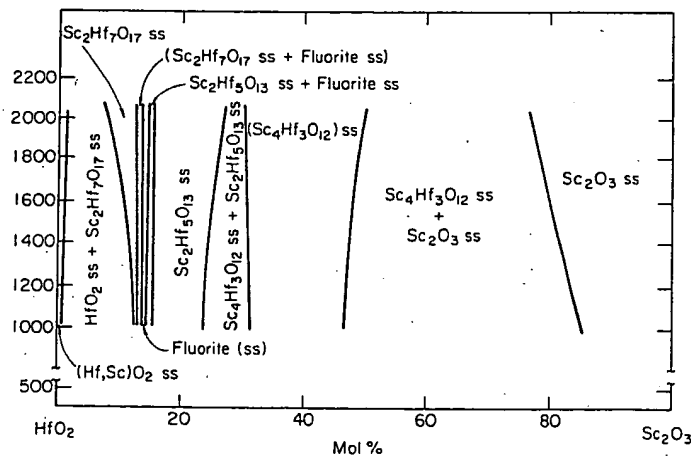
$$\text{R}_2\text{O}_3\text{-ZrO}_2$$


FIG. 5241.—System  $ZrO_2-R_2O_3$  (rare earth oxides).  
F. Sibieude and A. Rouanet, *Colloq. Int. CNRS*, 1972, No. 205, p. 459.

Results are given for a sequence of studies of the system  $\text{ZrO}_2\text{-R}_2\text{O}_3$  where  $\text{R} = \text{Yb, Y, Er, Ho, Dy, and Gd}$ , using solar furnace thermal equilibration analysis and high temperature X-ray powder diffraction. Liquidus curves were determined at 5 mol% intervals.

D.R.W.

$$\text{Sc}_2\text{O}_3\text{--HfO}_2$$


ide Systems

### Two Oxides

137

**Figs. 5239–5242**

BEST AVAILABLE COPY

**Nd<sub>2</sub>O<sub>3</sub>-ZrO<sub>2</sub> (concl.)**

The compound  $\text{Nd}_2\text{Zr}_2\text{O}_7$  does not retain its ordered structure to the melting point. The associated dashed line gives an estimated stability range for the ordered form assuming disorder above  $2300^\circ$  at the  $\text{Nd}_2\text{Zr}_2\text{O}_7$  composition. At this composition, the cooling curve<sup>1</sup> shows a thermal arrest at  $2250^\circ$ . This may reflect the order-disorder transition. At temperatures lower than  $2100^\circ$ , the solubility of  $\text{ZrO}_2$  and  $\text{Nd}_2\text{O}_3$  in  $\text{Nd}_2\text{Zr}_2\text{O}_7$  decreases giving two exsolution fields ( $P + C_1$  and  $P + C_2$ ).

In the zirconia-rich region the  $C_1$  phase is completely stabilized with an addition of 15 mol%  $Nd_2O_3$ . The  $T \rightarrow C_1$  transition is reversible. This diagram differs in detail from previous, incomplete diagrams (Figs. 350, 2382, 2383) but resembles most closely Fig. 2382. It should be considered the best diagram available. Future work should be performed to better define the immiscibility gaps and the  $C_1 \rightarrow P \rightarrow C_2$  transitions.

J. A. Rouanet, Thesis, 1970 reg. CNRS: A.O. 4239.

J.P.C.

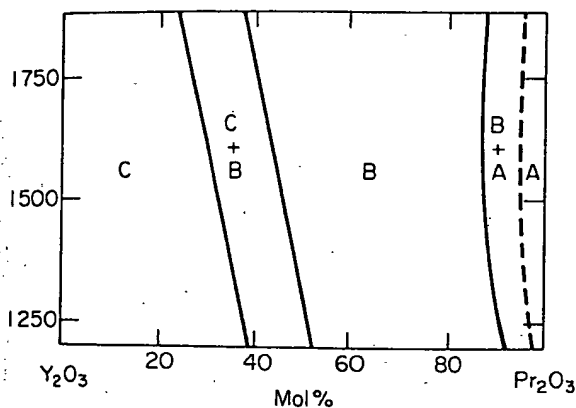
$$\text{Pr}_2\text{O}_3\text{-Y}_2\text{O}_3$$


FIG. 5240.—System  $Y_2O_3$ – $Pr_2O_3$ . C = cubic phase, B = monoclinic phase, A = hexagonal phase.

P. A. Tikhonov, K. Yu. Merezhinskii, and A. K. Kuznetsov, *Dokl. Akad. Nauk SSSR*, 222 [6] 1387 (1975); *Dokl. Phys. Chem. (Engl. Transl.)*, 222 [6] 650 (1975).

The starting materials consisted of 99.9%  $Y_2O_3$  and 99.8%  $Pr_6O_{11}$ . The oxides were mixed, pelletized, and heated at 1750° for 3 h in vacuum ( $10^{-1}$  mm Hg). Specimens were then heat-treated at 1250° (10 h), 1500° (5 h), and 1800° (2 h) in a vacuum of  $10^{-3}$  mm Hg, followed by quenching. Phases present were identified by X-ray diffraction.

Broad bands of solid solutions were found corresponding to the standard C and B forms of the rare earth oxide structures.<sup>1</sup> A narrow range of A-type solid solutions was found at high  $\text{Pr}_2\text{O}_3$  contents. Within the C and B structural types, the unit cell volume increased linearly with increasing mol%  $\text{Pr}_2\text{O}_3$ . The volume of the A unit cell also increased with increasing  $\text{Pr}_2\text{O}_3$  content, but only two points were determined.

The authors speculate that, while B forms for all rare earth oxides except  $Y_2O_3$  have been found at high pressures,<sup>2,3</sup> linear extrapolation of the B lattice parameters for  $Y_2O_3$ - $Pr_2O_3$  solid solutions to 0%  $Pr_2O_3$  is a valid method for estimating the lattice parameters for the as yet undiscovered B form of  $Y_2O_3$ .

1. J. D. McCullough and J. D. Britton, *J. Am. Chem. Soc.*, **74** [20] 5225 (1952).
2. H. R. Hoekstra and K. A. Gingerich, *Science*, **146** [3648] 1163 (1964).
3. H. R. Hoekstra, *Inorg. Chem.*, **5** [5] 754 (1966).

M.F.B:

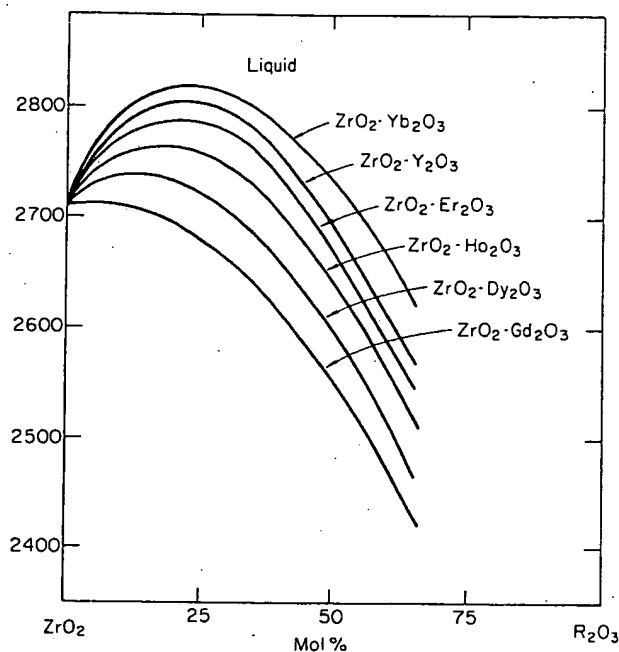
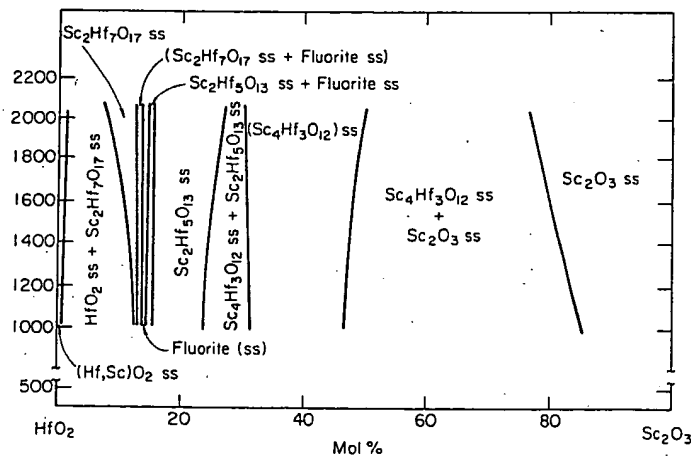
$$\text{R}_2\text{O}_3\text{-ZrO}_2$$


FIG. 5241.—System  $ZrO_2-R_2O_3$  (rare earth oxides).  
F. Sibieude and A. Rouanet, *Colloq. Int. CNRS*, 1972, No. 205, p. 459

Results are given for a sequence of studies of the system  $\text{ZrO}_2\text{-R}_2\text{O}_3$  where  $\text{R} = \text{Yb, Y, Er, Ho, Dy, and Gd}$ , using solar furnace thermal equilibration analysis and high temperature X-ray powder diffraction. Liquidus curves were determined at 5 mol% intervals.

D.R.W.

$$\text{Sc}_2\text{O}_3\text{-HfO}_2$$


# $\text{Sm}_2\text{O}_3\text{-ZrO}_2$ BEST AVAILABLE COPY

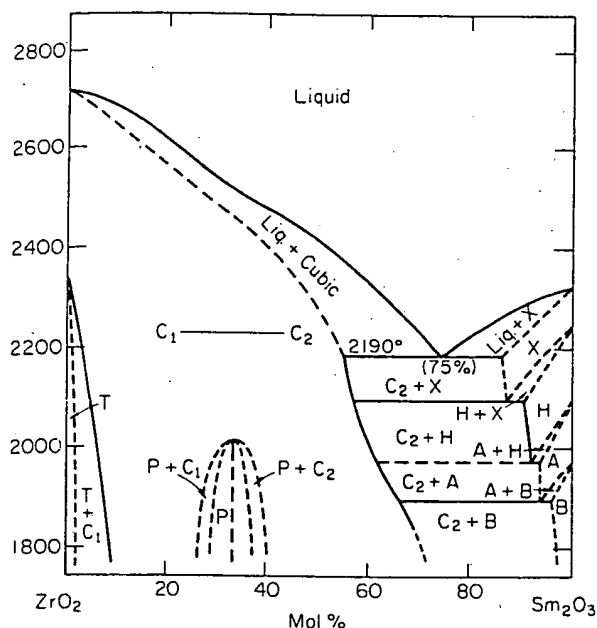


Fig. 5245.—System  $\text{ZrO}_2\text{-Sm}_2\text{O}_3$ . A, H = hexagonal ss, X = cubic ss, B = monoclinic ss,  $C_1$ ,  $C_2$  = cubic ss, P = pyrochlore phase, T = tetragonal ss.

A. Rouanet, *Rev. Int. Hautes Temp. Refract.*, 8 [2] 161 (1971).

The liquidus curve and phase transformations in the solid state were obtained by methods described in Fig. 5232. All dashed curves are estimated.  $\text{ZrO}_2$  (99.9, without  $\text{HfO}_2$ ) and  $\text{Sm}_2\text{O}_3$  (99.9) were the starting materials. For the polymorphism of  $\text{ZrO}_2$ , see Fig. 4259 and for  $\text{Sm}_2\text{O}_3$  Ref. 1.

The apparent inflection on the liquidus curve between  $\text{ZrO}_2$  and the eutectic is not explained but corresponds roughly to the pyrochlore (P) composition. It may reflect partial ordering in the liquid. The eutectic is at 25%  $\text{ZrO}_2$ -75%  $\text{Sm}_2\text{O}_3$ , 2190°.

On the rare earth-rich side, the X phase could not be quenched and is difficult to study at high temperature (>2100°) because of the high volatility of  $\text{Sm}_2\text{O}_3$ . Therefore, the homogeneity range of X could not be determined. The X→H transition temperature decreases sharply and the H→A transition is difficult to detect in solid solutions by thermal analysis.

The pyrochlore compound,  $\text{Sm}_2\text{Zr}_2\text{O}_7$ , disorders above 2000°. The author assumes that the  $C_1$  (cubic fluorite-type) →  $C_2$  (cubic  $\text{Ti}_2\text{O}_3$ -type) transition is continuous with a theoretical boundary at the pyrochlore composition. At the zirconia-rich side, the  $C_1$  phase is completely stabilized with ≈5%  $\text{Sm}_2\text{O}_3$ . The tetragonal (T) →  $C_1$  transition is reversible. The author states that near 6 to 7 mol%  $\text{Sm}_2\text{O}_3$  an inflection (not explained) appears on the T →  $C_1$  curve.

This diagram differs from Figs. 2387 and 4433, but is more consistent with Figs. 5232 and 5239. Because of polymorphism, the X, H, and A solid solutions of  $\text{Sm}_2\text{O}_3$  must show eutectoid decomposition giving, respectively,  $C_2 + \text{H}$ ,  $C_2 + \text{A}$ , and  $C_2 + \text{B}$ . The diagram is redrawn accordingly.

It appears that additional efforts must be made to obtain a better knowledge of this system especially at high temperature where a diphasic region  $C_1 + C_2$  must exist. Also, a reassessment of the  $\text{Sm}_2\text{O}_3$ -rich side is appropriate. In both cases, long term equilibration at elevated temperature will be necessary.

1. M. Foex and J. P. Traverse, *Rev. Int. Hautes Temp. Refract.*, 3 [4] 429 (1966).

# $\text{Sm}_2\text{O}_3\text{-MoO}_3$

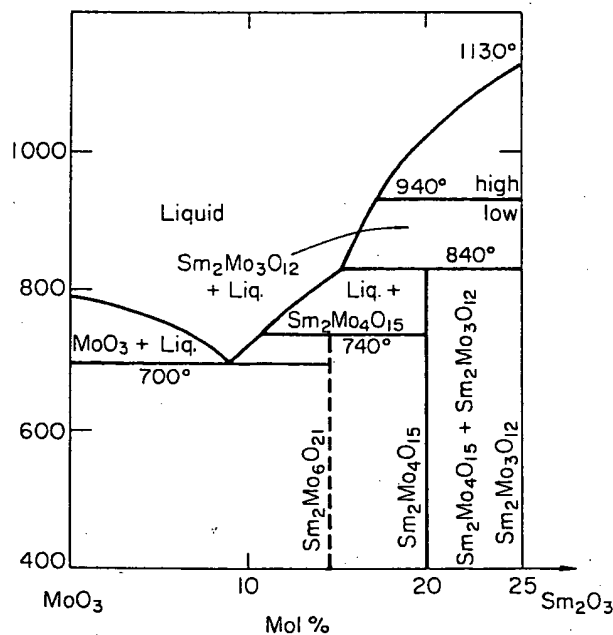


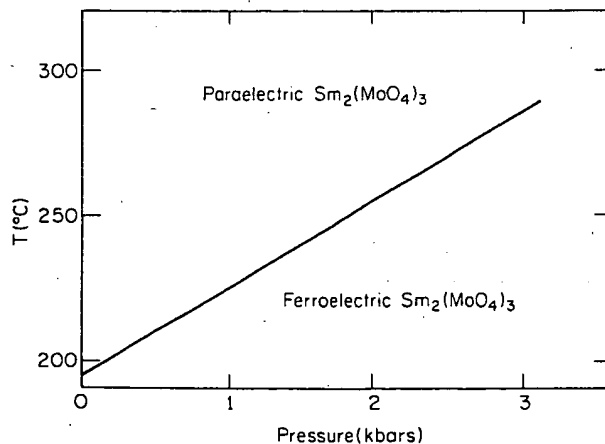
Fig. 5246.—System  $\text{MoO}_3\text{-Sm}_2\text{O}_3$ .

S. S. Antonova, I. V. Shakhno, V. E. Plyushchev, *Izv. Vyssh. Uchebn. Zaved., Khim. Khim. Tekhnol.*, 14 [1] 17 (1971).

Samples were prepared by prolonged heating and slow cooling of oxide mixtures in air at 500° to 650°. Analysis was by DTA and X-ray diffractometry. Unit cell parameters of the incongruent melting  $\text{Sm}_2\text{Mo}_4\text{O}_{15}$  (1:4) compound are listed. The 1:6 compound,  $\text{Sm}_2\text{Mo}_6\text{O}_{21}$ , was also identified and a unit cell reported. However, during 120 h heating periods at 720°, 20° below the DTA melting temperature, it was found to completely decompose into  $\text{MoO}_3$  and the 1:4 compound. The melting and/or decomposition of this phase is probably time dependent. Polymorphic transition of  $\text{Sm}_2\text{Mo}_3\text{O}_{12}$  at 940° was taken into consideration.

This system (at least the 1:6 compound) is qualitatively similar to the systems  $\text{MoO}_3\text{-Y}_2\text{O}_3$  and  $\text{MoO}_3\text{-Er}_2\text{O}_3$  described in the same reference (Figs. 5254 and 5218).

D.K.



1. M. Foex and J. P. Traverse, *Rev. Int. Hautes Temp. Refract.*, 3 [4] 429 (1966).

## BEST AVAILABLE COPY

 $Y_2O_3$ - $ThO_2$  (concl.)

FIG. 5250.—System  $ThO_2$ - $Y_2O_3$ . H = hexagonal (ss).  
F. Sibieude and M. Foex, *J. Nucl. Mater.*, 56 [2] 229 (1975).

The liquidus curves and phase transformations in the solid state were obtained by methods described in Fig. 5231. The diagram is tentative and based on experimental results obtained by thermal analysis and high temperature X-ray diffraction and on data for the polymorphism of  $Y_2O_3$ .<sup>1</sup> The liquidus curve is characterized by a eutectic in the  $Y_2O_3$ -rich side ( $\approx 15\%ThO_2$ -85% $Y_2O_3$ ) at  $\approx 2400^\circ$ .

This diagram resembles the system  $ThO_2$ - $Er_2O_3$  (Fig. 5215) except that the solution of  $ThO_2$  is greater in C- $Y_2O_3$  and smaller in H- $Y_2O_3$  than in C- $Er_2O_3$  and H- $Er_2O_3$ . The limits of  $Y_2O_3$  and  $ThO_2$  dissolution, respectively, in C- $ThO_2$  and C- $Y_2O_3$  differ from previous results (Fig. 2389). Because of the use of high temperature X-ray diffraction and thermal analysis, this diagram must be considered as the best available.

1. M. Foex and J. P. Traverse, *Rev. Int. Hautes Temp. Refract.*, 3 [4] 429 (1966). J.P.C.

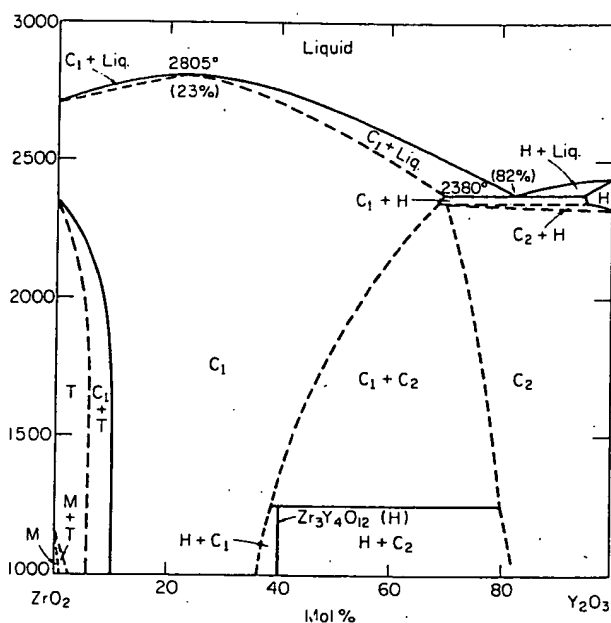
 $Y_2O_3$ - $ZrO_2$ 

FIG. 5251.—System  $ZrO_2$ - $Y_2O_3$ .  $C_1$  = cubic ss of the  $CaF_2$  type,  $C_2$  = cubic ss of the  $ThO_3$  type, H = hexagonal structure, T = tetragonal structure, M = monoclinic structure.

A. Rouanet, *Rev. Int. Hautes Temp. Refract.*, 8 [2] 161 (1971).  
S. R. Skaggs, Tech. Rept., SC-RR-72-0031, Jan. 1972, p. 89.

This system has been studied extensively by numerous workers, especially A. Rouanet and S. R. Skaggs, within the very high temperature range. Rouanet obtained liquidus curves and phase transitions by methods described in Fig. 5232. Skaggs melted samples by laser heating. In both studies liquidus temperatures were determined from cooling curves obtained using automatic pyrometers ( $0.65 \mu m$ ). Rouanet obtained cooling curves in good blackbody conditions. Melting points ( $Al_2O_3$ ,  $2054^\circ$ ;  $Y_2O_3$ ,  $2440^\circ$ ) provided standards for the pyrometer. Skaggs used published emissivity values (0.84 for  $ZrO_2$  and 0.96 for  $Y_2O_3$ ). Liquidus temperatures differ in some regions by more than  $100^\circ$ . Earlier diagrams (Figs. 4437(A) and (B)) show a liquidus maximum reported also by Noguchi.<sup>1</sup> After Rouanet, the composition and temperature of the liquidus maximum are, respectively, 77 mol%  $ZrO_2$ -23 mol%  $Y_2O_3$  and

$2805^\circ$ . The solidus curve of Skaggs is inconsistent with the liquidus maximum, illustrating the difficulty of good temperature measurements at extreme temperatures.

Other differences are evident between the two diagrams; (1) at the yttrium oxide-rich side, the cubic ( $C_2 \rightarrow$  hexagonal H) phase transition ( $T = 2330^\circ$ )<sup>2</sup> is not shown, (2) Rouanet found a eutectic ( $2380^\circ$ , 18 mol%  $ZrO_2$  - 82 mol%  $Y_2O_3$ ) and Skaggs a peritectic ( $2483^\circ$ , same composition), and (3) the major conflict is the existence of a two-phase region between the cubic fluorite-type solid solution ( $C_1$ ) and the cubic  $ThO_3$ -type solid solution ( $C_2$ ).

In both studies, the pyrochlore compound ( $Y_2Zr_2O_7$ ) postulated in Fig. 2390 was not found. Recently, Ref. 3 has shown that long time annealing (2 weeks,  $\approx 1200^\circ$ ) of  $2ZrO_2 \cdot Y_2O_3$  mixtures does not yield the ordered pyrochlore compound. However, the hexagonal compound,  $Zr_3Y_4O_{12}$ , was found, which decomposes above  $1250^\circ \pm 60^\circ$ .

Using the data of Rouanet and Skaggs, and of Refs. 3 to 5, this tentative diagram was constructed by the compiler (see also Fig. 5252). Additional studies are required to delimit such biphasic regions as  $C_1 + C_2$ ,  $C_1 + H$ ,  $C_2 + H$  (H, ordered compound,  $Zr_3Y_4O_{12}$ ). Liquidus curves are after Rouanet.

1. T. Noguchi; p. 249 in *Advances in High Temperature Chemistry*, Vol. 2. Edited by L. Eyring, Academic Press, New York, 1969.
2. M. Foex and J. P. Traverse, *Rev. Int. Hautes Temp. Refract.*, 3 [4] 429 (1966).
3. S. P. Ray and V. S. Stubican, *Mater. Res. Bull.*, 12 [5] 549 (1977).
4. R. Ruh, K. S. Mazdhyasni, and H. O. Bielstein; presented at the 70th Annual Meeting, The American Ceramic Society, Chicago, Ill., May 1968. (Basic Science Div. No. 65-B-68; for abstract see *Am. Ceram. Soc. Bull.*, 47 [4] 366 (1968).
5. O. Sardi, Ph.D. Thesis, University of Indiana (1969). J.P.C.

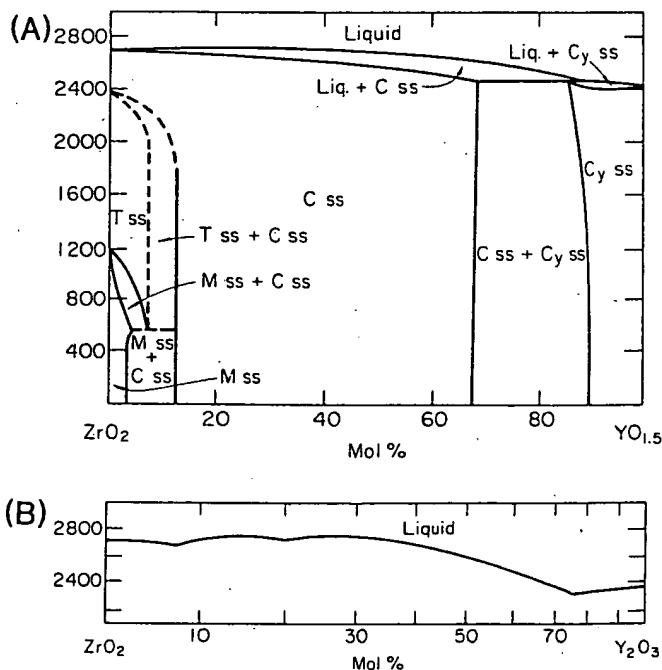


FIG. 5252.—System  $ZrO_2$ - $YO_{1.5}$ . (A) Composite diagram, (B) liquidus curve from Ref. 2.

K. K. Srivastava, R. N. Patil, C. B. Choudhary, K. V. G. K. Gokhale, and E. C. Subbarao, *Trans. J. Br. Ceram. Soc.*, 73 [3] 85 (1974).

Twenty compositions across the entire system were prepared at  $2000^\circ$  using an oxyacetylene furnace. Analysis was by subsequent X-ray diffraction at room temperature. Quantitative DTA was used to observe transformations. The experimental results confirm a

**Yb<sub>2</sub>O<sub>3</sub>-HfO<sub>2</sub> (concl.)**

FIG. 5255.—System HfO<sub>2</sub>-Yb<sub>2</sub>O<sub>3</sub>. C = Ti<sub>2</sub>O<sub>3</sub>-type structure, F = fluorite-type structure.

E. B. Perova, A. A. Samoilenko, F. M. Spiridonov, L. N. Komissarova, *Zh. Neorg. Khim.*, 17 [10] 2846 (1972); *Russ. J. Inorg. Chem. (Engl. Transl.)*, 17 [10] 1492 (1972).

This system was examined from 1000° to 1800° by X-ray diffraction. Samples were coprecipitated and prepared at 2 to 2.5 mol% intervals across the system. No compounds were observed, all solid solutions are cubic, the C being Ti<sub>2</sub>O<sub>3</sub>-type, the F being fluorite-type. A linear relation was found between the lattice parameters of the solid solutions and the composition at the various annealing temperatures. The monoclinic-tetragonal phase transition is not shown for HfO<sub>2</sub> ss.

D.R.W.

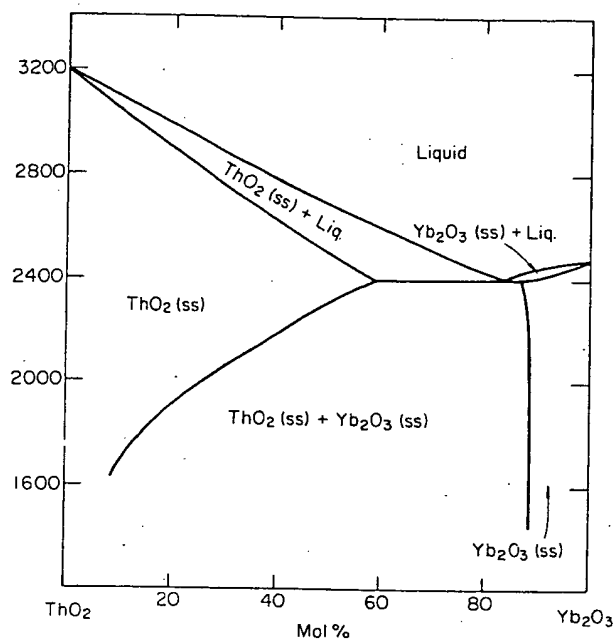
**Yb<sub>2</sub>O<sub>3</sub>-ThO<sub>2</sub>**

FIG. 5256.—System ThO<sub>2</sub>-Yb<sub>2</sub>O<sub>3</sub>.

F. Sibieude and M. Foex, *J. Nucl. Mater.*, 56 [2] 229 (1975).

The liquidus curve was obtained by methods described in Fig. 5231. This diagram is tentative and based on experimental results obtained by thermal analysis and high temperature X-ray diffraction. The solidus and liquidus curves between ThO<sub>2</sub> and 55% ThO<sub>2</sub>-45% Yb<sub>2</sub>O<sub>3</sub> are estimated.

The liquidus curve is characterized by a eutectic on the Yb<sub>2</sub>O<sub>3</sub>-rich side (≈15% ThO<sub>2</sub>-85% Yb<sub>2</sub>O<sub>3</sub>) at 2400°.

The only solid phases are cubic ThO<sub>2</sub> and cubic Yb<sub>2</sub>O<sub>3</sub>. On the Yb<sub>2</sub>O<sub>3</sub>-rich side the solubility of C-ThO<sub>2</sub> in C-Yb<sub>2</sub>O<sub>3</sub> is independent of the temperature: 10 mol% C-ThO<sub>2</sub> in C-Yb<sub>2</sub>O<sub>3</sub> between 1400° and 2200°. On the thoria-rich side the solubility of C-Yb<sub>2</sub>O<sub>3</sub> increases from 10% at 1600° to 60% at 2400°.

J.P.C.

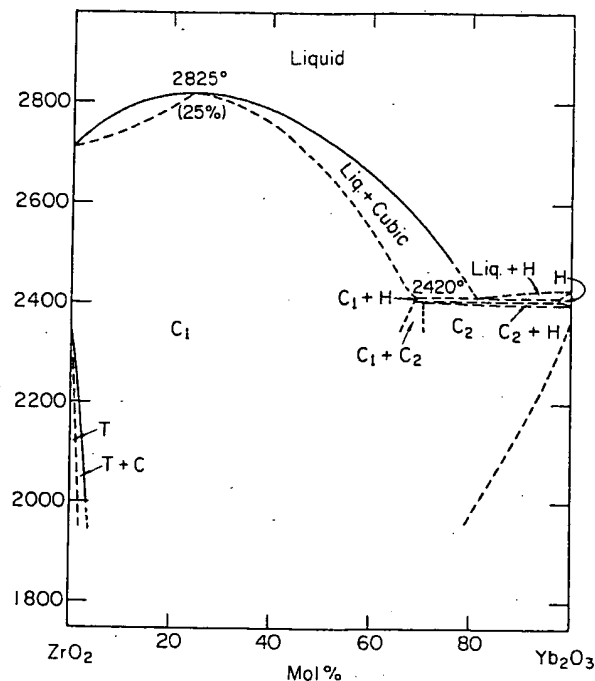
**Yb<sub>2</sub>O<sub>3</sub>-ZrO<sub>2</sub>**

FIG. 5257.—System ZrO<sub>2</sub>-Yb<sub>2</sub>O<sub>3</sub>. H = hexagonal ss, C<sub>1</sub> and C<sub>2</sub> = cubic ss phases, T = tetragonal ss.

A. Rouanet, *Rev. Int. Hautes Temp. Refract.*, 8 [2] 161 (1971).

The liquidus curve was obtained by the thermal analysis device described in Fig. 5232. All dashed curves are estimated. ZrO<sub>2</sub> (99.9% without HfO<sub>2</sub>) and Yb<sub>2</sub>O<sub>3</sub> (99.9%) were the starting materials. On the zirconia-rich side, the tetragonal (T) → C<sub>1</sub> transition is reversible.

At high temperature (>1800°), solid solutions vary from a cubic fluorite structure (C<sub>1</sub>) to a cubic Ti<sub>2</sub>O<sub>3</sub>-type structure (C<sub>2</sub>). The author states that the theoretical boundary is at the ZrO<sub>2</sub>:Yb<sub>2</sub>O<sub>3</sub> composition but this is questionable. A biphasic region, C<sub>1</sub> + C<sub>2</sub>, must exist but it may be difficult to determine (e.g. sluggish solid state reactions). The dashed line at the Yb<sub>2</sub>O<sub>3</sub>-rich side reflects a thermal effect attributed by the author to the dissociation of Yb<sub>2</sub>O<sub>3</sub>. The ordered compound Zr<sub>3</sub>Yb<sub>4</sub>O<sub>12</sub><sup>1</sup> was not observed, perhaps due to the low temperature limit of this study (≈1800°).

By carefully studying cooling curves of Yb<sub>2</sub>O<sub>3</sub>, Traverse<sup>2</sup> suggested that a C→H phase transition could exist just below the melting point. This diagram represents a tentative revision of Fig. 4440.

1. M. R. Thornber and D. J. M. Bevan, *J. Solid State Chem.*, 1 [3-4] 536 (1970).

2. J. P. Traverse, Thesis, CNRS, AO5879, June 1971. J.P.C.

**MgO-CeO<sub>2</sub>-ZrO<sub>2</sub> (concl.)**

FIG. 5418.—System CeO<sub>2</sub>-MgO-ZrO<sub>2</sub>. (A) 1700° section, (B) 1500° section, (C) 1300° section, (D) 1200° section.

V. Longo and L. Podda, *Ceramurgia*, 1 [2] 92 (1971).

At least 227 compositions were formulated from CeO<sub>2</sub> (99.9%), MgCO<sub>3</sub> (99.8%), and ZrO<sub>2</sub> (99.7%, excluding ≈2% HfO<sub>2</sub>). These were pressed into disks and fired in air according to the following schedules:

- (a) 1400°, 250 h, then 8 h at 1600° and 1700°
- (b) 1400°, 500 h, then 150 h at 1500°
- (c) 1400°, 750 h, then 1000 h at 1400° and 1200 h at 1300°
- (d) 1400°, 1000 h, then 1200°, 1500 h, and 1100°, 1500 h

Temperature was measured by calibrated Pt-Pt10Rh thermocouples. More than 1000 samples (quenched in air) were analyzed by reflected light microscopy and powder X-ray diffraction and sections for the 1700°, 1600°, 1500°, 1400°, 1300°, 1200°, and 1100° isotherms were constructed accordingly. Only four of these sections deemed sufficiently different are included here.

CeO<sub>2</sub> accepts little MgO in solid solution. The extent of a tetragonal ZrO<sub>2</sub> solid solution with MgO is considered minimal in general accord with Fig. 4339 but not with Figs. 271 and 2317. With decreasing temperature, the ternary cubic solid solution field progressively decreases in extent until equilibria are dominated by the binary phase assemblages.

These isothermal sections were constructed, apparently assuming that cerium remains 4+ (i.e. CeO<sub>2</sub>) within binary and ternary solid solutions. Reduction of some of the cerium to 3+ is probable at the elevated temperatures, and, hence, these sections must be considered as isobaric-isothermal equilibria in the system CeO<sub>2</sub>-Ce<sub>2</sub>O<sub>3</sub>-MgO-ZrO<sub>2</sub> projected onto the CeO<sub>2</sub>-MgO-ZrO<sub>2</sub> plane. T.N.

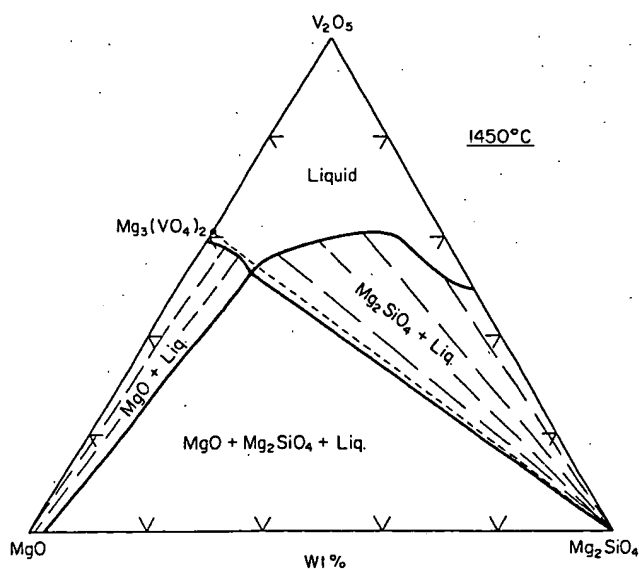
**MgO-SiO<sub>2</sub>-V<sub>2</sub>O<sub>5</sub>**

FIG. 5419.—System MgO-Mg<sub>2</sub>SiO<sub>4</sub>-V<sub>2</sub>O<sub>5</sub> 1450° section.

M. Carter and N. H. Brett, *Trans. J. Br. Ceram. Soc.*, 72 [5] 203 (1973).

More than fifty compositions were reacted in the solid state and when liquid was present they were quenched. Experimental methods are described in the commentary for Fig. 5486. This isothermal section illustrates the effect of V<sub>2</sub>O<sub>5</sub> on refractories based on MgO and Mg<sub>2</sub>SiO<sub>4</sub> (forsterite). The location of the 1450° isotherm and its intersection with the MgO-Mg<sub>2</sub>SiO<sub>4</sub>-liquid boundary curve yields a ternary point given at 39% MgO, 11% M<sub>2</sub>S, and 50 wt% V<sub>2</sub>O<sub>5</sub>. See Figs. 5485 and 5486 for additional aspects of this work. T.N.

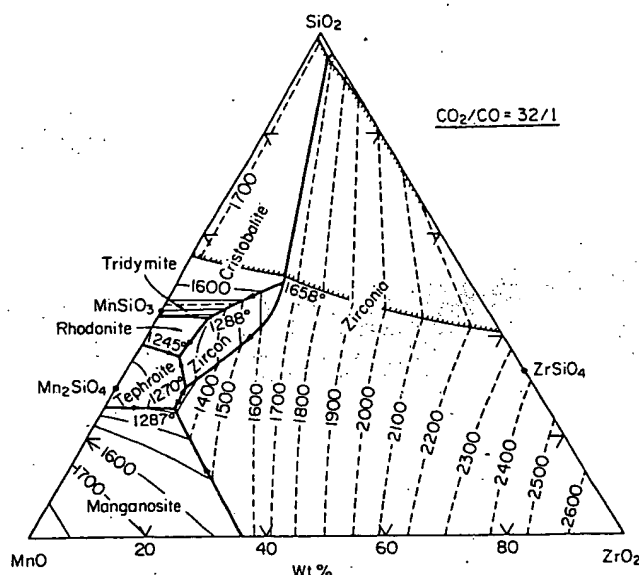
**MnO-SiO<sub>2</sub>-ZrO<sub>2</sub>**

FIG. 5420.—System MnO-ZrO<sub>2</sub>-SiO<sub>2</sub>.

R. L. Shultz and A. Muan, *J. Am. Ceram. Soc.*, 54 [10] 504 (1971).

Phase relations in the liquidus region of the system MnO-ZrO<sub>2</sub>-SiO<sub>2</sub> were determined by the quenching technique. Starting mixtures were prepared from high-purity chemicals heated at 1400° (air, 12 h) within Mn-saturated Pt crucibles. The glassy products were then homogenized and treated at 1200° (air, 48 h) and at 1150° (a reducing atmosphere, 48 h). Pressed pellets wrapped with fine Pt wire were equilibrated at sufficiently low oxygen pressures (CO<sub>2</sub>-CO atmospheres of controlled CO<sub>2</sub>/CO ratios) to keep most of the Mn in the divalent state. Calibrated Pt-PtRh thermocouples were used to measure temperature with an estimated accuracy of ±5°. Phase assemblages of the quenched samples were determined by microscopic and X-ray examination.

The diagram shows the liquidus surface of the system in a CO<sub>2</sub>-CO atmosphere of CO<sub>2</sub>/CO ratio = 32/1. Heavy lines are boundary curves between adjacent primary phase areas, as labelled on the diagram; light lines are liquidus isotherms, and lines with shading on one side are outlines of a two-liquid region. The system is not strictly ternary as the oxidation state of Mn is variable. Nevertheless, "invariant" points are generated by the intersections of univariant boundary curves and the oxygen isobaric section. These ternary invariant points are summarized below.

Temp. (°C)	Phases + liquid	Liquid composition (wt%)		
		MnO	ZrO <sub>2</sub>	SiO <sub>2</sub>
1287	Mn <sub>2</sub> SiO <sub>4</sub> , MnO, ZrO <sub>2</sub>	62	12	26
1270	Mn <sub>2</sub> SiO <sub>4</sub> , ZrO <sub>2</sub> , ZrSiO <sub>4</sub>	58	12	30
1245	Mn <sub>2</sub> SiO <sub>4</sub> , ZrSiO <sub>4</sub> , MnSiO <sub>3</sub>	56	8	36
1288	ZrSiO <sub>4</sub> , MnSiO <sub>3</sub> , SiO <sub>2</sub>	47	9	44
1658	ZrSiO <sub>4</sub> , ZrO <sub>2</sub> , SiO <sub>2</sub>	31	19	50
1670	ZrSiO <sub>4</sub> , SiO <sub>2</sub>	30	19	51
	two liquids	1	4	95

A.M.

ZnO-SiO<sub>2</sub>-Nb<sub>2</sub>O<sub>5</sub> (concl.)

FIG. 5436.—System ZnO-SiO<sub>2</sub>-Nb<sub>2</sub>O<sub>5</sub>. Z = ZnO, N = Nb<sub>2</sub>O<sub>5</sub>, S = SiO<sub>2</sub>, ZN = ZnPb<sub>2</sub>O<sub>6</sub>, Z<sub>3</sub>N = ZnPb<sub>3</sub>O<sub>8</sub>, Z<sub>2</sub>S = ZnPb<sub>2</sub>SiO<sub>4</sub>, Z<sub>2</sub>N<sub>17</sub> = ZnPb<sub>2</sub>Nb<sub>34</sub>O<sub>87</sub>. Ternary liquidus diagram (A) and binary systems Z<sub>3</sub>N - Z<sub>2</sub>S (B), ZN - Z<sub>2</sub>S (C), and ZN - S (D). (E) and (F) show subsolidus tie lines at 1000° to 1085° and 1085° to 1200°, respectively.

R. R. Dayal, *J. Less-Common Met.*, 29 [1] 1 (1972).

The ternary system ZnO-Nb<sub>2</sub>O<sub>5</sub>-SiO<sub>2</sub> was studied using hot-stage microscopy (liquidus region) and quenching (subsolidus region) techniques. Oxide mixtures were prepared for study by grinding under acetone and firing at 1000° for 18 h with successive homogenization. Liquidus temperatures were reported to be accurate to ±5°. Subsolidus charges were held for an unspecified duration in a platinum tube furnace and quenched in air for later X-ray diffraction identification. Pertinent details concerning the liquidus phase relations are given in the table:

Composition (wt%)*			Temp. (°C)	Phases present
ZnO	Nb <sub>2</sub> O <sub>5</sub>	SiO <sub>2</sub>		
53.0	43.8	3.2	1248	Z + Z <sub>3</sub> N + α-Z <sub>2</sub> S + liquid
48.0	46.5	5.5	1244	Z <sub>3</sub> N + α-ZN + Z <sub>2</sub> S + liquid
44.0	41.5	14.5	1264	Z <sub>2</sub> S + α-ZN + S + liquid
17.0	79.0	4.0	1352	β-ZN + Z <sub>2</sub> N <sub>17</sub> + S + liquid
9.8	88.0	2.2	1407	Z <sub>2</sub> N <sub>17</sub> + N + S + liquid

\*All compositions listed were eutectic type.

C.E.S.

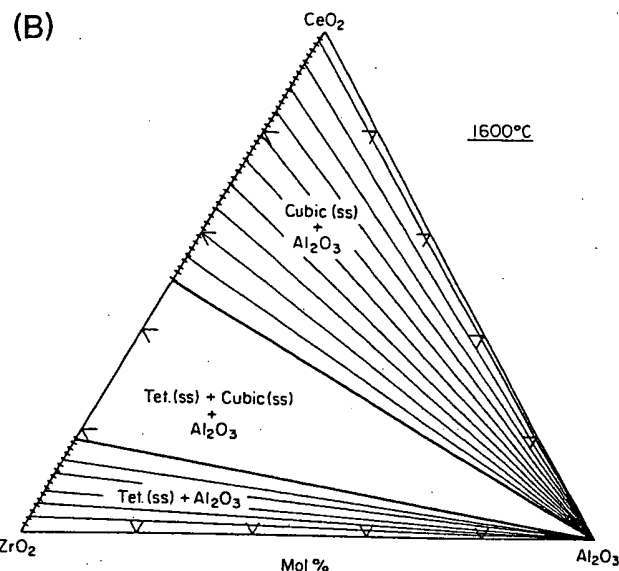
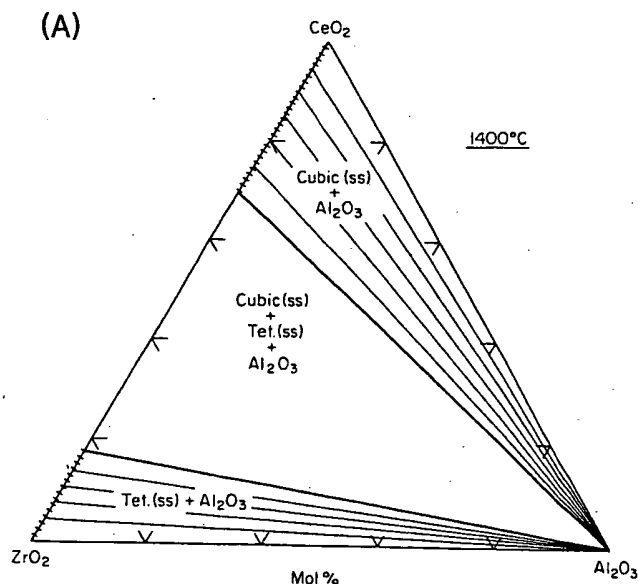
Al<sub>2</sub>O<sub>3</sub>-CeO<sub>2</sub>-ZrO<sub>2</sub>

FIG. 5437.—System ZrO<sub>2</sub>-Al<sub>2</sub>O<sub>3</sub>-CeO<sub>2</sub>. (A) Subsolidus isothermal sections at 1400°. (B) Subsolidus isothermal sections at 1600°. V. Longo and L. Podda, *Ceramurgia*, 1 [1] 11 (1971).

More than 200 specimens were formulated from ZrO<sub>2</sub>, CeO<sub>2</sub>, and Al<sub>2</sub>O<sub>3</sub>, all having a stated purity of >99.8% excluding ≈2% HfO<sub>2</sub> in the former. These were mixed, pressed into disks, and fired in air at 1400° (1000 h) and at 1500° (250 h) followed by 1600° (8 h). Specimens were quenched in air and analyzed by reflected light microscopy and X-ray powder diffraction.

Diagrams (A) and (B) show subsolidus isothermal sections at 1400° and 1600°, respectively. Mutual solid solubility between Al<sub>2</sub>O<sub>3</sub> and ZrO<sub>2</sub> could not be detected at the 1 mol% level in agreement with Figs. 4377 and 4378. ZrO<sub>2</sub>-Al<sub>2</sub>O<sub>3</sub> specimens did not melt up to 1730°, suggesting a solidus temperature higher than that given in Fig. 4377. Solid solution in the system CeO<sub>2</sub>-Al<sub>2</sub>O<sub>3</sub> also was not detected. However above 1600° in air (and at lower temperatures at lower P<sub>O2</sub>) the compounds Ce<sup>3+</sup>AlO<sub>3</sub> and Ce<sub>2</sub>O<sub>3</sub>·11Al<sub>2</sub>O<sub>3</sub> are reported to be stable.

These isothermal sections were constructed, apparently assuming that CeO<sub>2</sub> and "CeO<sub>2</sub>"/ZrO<sub>2</sub> solid solutions are stoichiometric. CeO<sub>2</sub>, however, undergoes slight reduction at high temperatures even in air (e.g. Ref. 1). "CeO<sub>2</sub>"/ZrO<sub>2</sub> solid solutions undergo more substantial reduction in air (e.g. Ref. 2). Thus, these sections must be considered as isobaric-isothermal equilibria in the system CeO<sub>2</sub>-Ce<sub>2</sub>O<sub>3</sub>-Al<sub>2</sub>O<sub>3</sub>-ZrO<sub>2</sub> projected onto the CeO<sub>2</sub>-Al<sub>2</sub>O<sub>3</sub>-ZrO<sub>2</sub> plane.

1. R. J. Panlener and R. N. Blumenthal, AEC Report 000-1441-18 (1972).
2. T. Negas, R. S. Roth, C. L. McDaniel, H. S. Parker, and C. D. Olson, *Proc. Rare Earth Res. Conf.*, 12th, 2, 605 (1976). Edited by C. E. Lundin.

T.N.

BEST AVAILABLE COPY